International Journal of Hydrogen Energy 231 (2026) 154958

Contents lists available at ScienceDirect

International Journal of Hydrogen Energy

journal homepage: www.elsevier.com/locate/he

Techno-economic assessment of the sorption enhanced methanation: Levelized cost of methane, performance indicators and sensitivity analysis

C. Barón [a], L. Gómez [b], I. Martínez [b], M. Bailera [a,*]

[a] Energy and CO_2 Group, Aragon Institute of Engineering Research (I3A), Department of Mechanical Engineering, Escuela de Ingeniería y Arquitectura, Universidad de Zaragoza, María de Luna 3, 50018, Zaragoza, Spain
[b] Environmental Research Group, Instituto de Carboquímica (Spanish National Research Council, ICB-CSIC), Miguel Luesma Castán 4, 50018, Zaragoza, Spain

ARTICLE INFO

Keywords:
Sorption-enhanced methanation
Levelized-cost
Techno-economic assessment
Industrial decarbonization

ABSTRACT

This work presents the first techno-economic assessment of sorption-enhanced methanation (SEM) based on TRL-3 experimental data, comparing it with conventional methanation (CM). Experimental tests fitted a kinetic model for reactor sizing in a 200 MW_e plant. While SEM requires more catalyst (223.7 kg/MW_e) than CM (70–90 kg/MW_e), both systems show similar CAPEX (~700-800 M€). The results highlight that SEM generates three times higher income due to superior product purity. Conventional methanation often faces economic losses when producing 95% CH_4, as levelized costs (LCOM, 2.4 – 3.3 €/kg) exceed market prices (0.5 €/kg). Although CM can be profitable at 99% purity market, SEM achieves 99.9% CH_4, accessing a premium market (12 €/kg) that guarantees profitability even in unfavorable hydrogen cost scenarios. Consequently, SEM emerges as a key technology to enhance the economic viability and maturity of innovative H_2 production.

1. Introduction

Climate change and the depletion of natural resources are among the most urgent and formidable challenges facing modern science [1]. Carbon dioxide (CO_2) is a primary driver of global climate change, and with a growing world population and the accelerating industrialization of developing nations, immediate and effective strategies are essential to limit its impact [2,3]. In this context, CO_2 utilization has gained significant attention as a promising approach, enabling the conversion of these CO_2 emissions into valuable fuels and chemicals, thereby mitigating resource depletion [4]. This approach has several advantages over conventional strategies such as carbon capture and storage [5,6]. At the same time, fossil fuels are becoming increasingly scarce and environmentally unsustainable. This creates two critical challenges: replacing fossil fuels as primary energy sources while ensuring compatibility with existing end-use applications, and expanding energy storage capacity to manage the intermittency of renewable power generation [7]. The European Green Deal has established a bold roadmap to address these challenges and achieve net-zero greenhouse gas emissions by 2050, prioritizing renewable energy deployment and industrial decarbonization [8].

Power-to-Gas (PtG) technology directly addresses these needs [9]. Among the different PtG approaches, the production of synthetic methane has emerged as a leading option in recent years. This process involves producing hydrogen via water electrolysis using surplus renewable electricity, which is then reacted with captured CO_2 to generate synthetic methane through methanation reactions (Eqs. (1) and (2)) [10,11]. PtG technology effectively links the electricity and gas networks, enabling the storage of excess renewable power for later use in meeting backup or end-use energy demand. The required carbon feedstock is supplied by obtaining CO_2 through carbon capture technologies, where it is valorized rather than stored, thus reducing the need for dedicated sequestration. The resulting synthetic methane can be transported through the existing gas infrastructure and consumed directly by industry, households, buildings and transport, displacing fossil fuels in applications where alternative renewable solutions are difficult to implement [12,13].

$$CO_2 + 4H_2 \leftrightarrow CH_4 + 2H_2O \quad \Delta H^{\circ}_{298} = -165\ kJ\ mol^{-1} \tag{1}$$

$$CO + 3H_2 \leftrightarrow CH_4 + H_2O \quad \Delta H^{\circ}_{298} = -206\ kJ\ mol^{-1} \tag{2}$$

Traditionally, methanation has been carried out using conventional processes involving a series of adiabatic fixed-bed reactors, with intermediate stages for cooling the gas and/or recycling the product, in order

* Corresponding author.
E-mail address: mbailera@unizar.es (M. Bailera).

https://doi.org/10.1016/j.ijhydene.2026.154958
Received 13 January 2026; Received in revised form 23 March 2026; Accepted 8 April 2026
Available online 11 April 2026

to control the maximum temperature reached [9]. These systems typically operate at temperatures between 250 °C and 450 °C, or up to approximately 700 °C when more robust catalysts are used, and at pressures exceeding 20 bar [14,15]. Such conditions favor methane formation because the exothermic nature of the reaction makes it thermodynamically favorable at low temperatures and high pressures [16]. However, operating at excessively high temperatures can accelerate catalyst deactivation due to thermal stress, while operating at excessively low temperatures can impose kinetic limitations [17,18]. To address these constraints, research efforts have primarily focused on two strategies: developing more active catalysts to enable efficient operation at lower temperatures [19–21] and designing advanced reactor configurations to manage the significant heat released by the methanation reaction more effectively [14,22,23]. Nevertheless, over the past decade, an alternative process intensification strategy has emerged as a promising approach to moving beyond conventional methanation. This approach, known as Sorption-Enhanced Methanation (SEM), integrates the reaction and separation processes in a single step, offering new opportunities to overcome the thermodynamic and kinetic limitations inherent in traditional systems [24–26].

The SEM process combines CO_2 methanation with in-situ H_2O removal by incorporating a solid sorbent into the reactor. According to *Le Chatelier's* principle, the continuous adsorption of the formed H_2O shifts the equilibrium towards CH_4 production. This results in higher conversions and methane yields under milder operating conditions [27,28]. In addition to improving equilibrium performance, in-situ H_2O capture mitigates catalyst deactivation, which is often accelerated by steam [27]. As H_2O adsorption is exothermic, it is thermodynamically favored at low temperatures. However, excessively low temperatures can hinder methanation kinetics, highlighting the need to balance between reaction and sorption conditions [29,30]. Zeolites are the most widely used sorbent materials in the SEM process due to their high water-adsorption capacity, thermal stability, and established use in industrial applications such as ethanol dehydration and flue gas [31,32]. In this process, zeolites are typically combined with methanation catalysts to promote CO_2 conversion and selectively capture the H_2O by-product simultaneously, enabling the production of high-purity synthetic natural gas (SNG) at relatively low temperatures [28]. Two main strategies can be distinguished in the literature: (i) modifying zeolites to introduce catalytic activity while retaining sufficient adsorption capacity [24,33,34], and (ii) physically combining active methanation catalysts, such as Ni-based materials, with zeolites acting as selective adsorbents [28,35–37]. Both approaches have demonstrated improved process performance, emphasizing the importance of zeolite–catalyst systems in advancing SEM technology.

The feasibility of the SEM concept has already been demonstrated experimentally both at laboratory scale [28,38] and at TRL-3 [39,40] levels. It has been shown that a pure CH_4 stream can be produced over a limited time period. This corresponds to the time during which the zeolite selectively adsorbs the formed H_2O. Once the sorbent is saturated, the process reverts to conventional methanation. To enable continuous CH_4 production, multiple reactors would need to operate in parallel, allowing for sorbent regeneration without interrupting the continuous production of methane [39].

From a technical perspective, the SEM concept presents, at the very least, potential to become an important driver for carbon valorization, thanks to overcoming the thermodynamic limits established by *Le Chatelier's* principle. Nonetheless, whether this technology will be deemed uncompetitive, coexist with, or even replace conventional methanation must be also answered in economic terms. In plain words, the most profitable technology will become the most relevant one.

This work presents the techno-economic assessment of the SEM process. The simulations are based on experimental data obtained under different operating conditions and are benchmarked against conventional methanation. To the best of our knowledge, this study is the first to provide a techno-economic evaluation of SEM, offering a direct comparison with conventional methanation under identical operating conditions and valuable insights into its industrial feasibility as a means of producing large quantities of synthetic methane. Moreover, it is the first study to provide the levelized cost of methane for SEM processes.

2. Case studies

A techno-economic comparison between the SEM and the conventional methanation processes will be performed. These technologies will be modelled in Aspen Plus based on experimental data. Then, valuable insights such as the mass of catalyst needed, the case-specific thermal integration performed and the economic revenue will be extracted.

The sorption-enhanced methanation concept is explained in section 2.1, whereas different configurations of conventional methanation are explained in section 2.2. For all cases, a mixture of 60 vol% CO and 40 vol% CO_2 is converted into CH_4 by using the corresponding stoichiometric amount of H_2. This flue gas, with 1.55 CO/CO_2 molar ratio or higher, is typical of the ironmaking industry. For example, gases with similar composition are found in basic oxygen furnaces [41], smelting reduction processes [42,43] and electric arc furnaces [44]. Therefore, this techno-economic assessment is of interest for industrial decarbonization.

For the conventional methanation process, purities of 95% and 99% will be obtained, whereas for SEM it is 100% (assumed 99.99%). The market changes according to the purity. The 95% presents the same use as user-grade natural gas [45]. The 99% may be used as feedstock for the chemical sector (i.e. for ammonia production) or in the transportation sector (liquid-SNG) [46]. The 99.9% presents applications either as calibration gas [47], in the semiconductor industry or fuel cells to prevent inconvenient depositions [48], or even as aerospace fuel [49]. For comparison purposes, a 1 MW_e PEM electrolyzer was considered (4.4 kWh/Nm^3 consumption, producing 20.4 kg/h of hydrogen) [50], due to its improved dynamic response and improved energy density and design compared to an AEL, all while presenting a higher maturity than SOEC. This means that the inlet flows of CO and CO_2 are 52.58 and 50.34 kg/h, respectively (0.11 mol of CO_2 and 0.18 mol of CO per total feed of stoichiometric H_2).

As a final consideration, it must be stated that, in this study, no impurities were considered. Each process would present a specific purification stage to deal with the specific impurities present in each CO/CO_2 gas source, with different compositions, technologies, and specific costs. Additionally, the steelmaking plant may (or not) already include a purification stage to comply with regulatory constraints. Taking all of that into account, feed gas purification has been considered out of the scope in this study, as it would restrict the results to a very specific utilization scenario, which is not the message we wanted to convey in this first-of-a-kind TEA for SEM.

2.1. Sorption-enhanced methanation

The SEM is based on the operation of a reactor filled with both catalyst and adsorbent, alternating methanation and regeneration stages (Fig. 1). In the methanation stage, the adsorbent traps the water produced during methanation, shifting the equilibrium towards CH_4 formation. During the regeneration phase, water is desorbed. A continuous SNG stream can be obtained when several reactors operating in parallel are considered. When one reactor is performing methanation, the others are desorbing water. For this case study, a setup with four reactors is considered, where methanation and regeneration take 15 and 45 min, respectively. An adsorbent/catalyst mass ratio of 4 is assumed for the reactors, which is reasonable considering recent published data on SEM [39,40]. The methanation reactor operates at 10 bar and 240 °C under stoichiometric $H_2/CO/CO_2$ feed gas conditions. The work of the compressor would be theoretically sufficient to heat the gas to the inlet temperature. However, an operation limit of 200 °C has been established to prevent damage to the equipment. Therefore, the last 200 to 240 °C

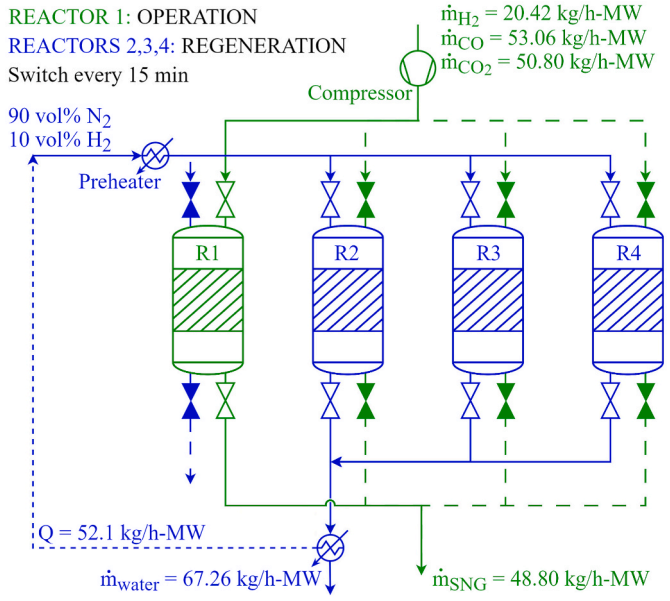

Fig. 1. Process flow diagram of a four-reactor sorption-enhanced methanation system.

are provided by electricity. The regeneration phase operates at 1 bar and 225 °C by flushing a gas with 90 vol% N_2 and 10 vol% H_2 (the required temperature is achieved by heat integration). The water content of the regeneration gas is condensed to recycle the N_2–H_2 part. This case study is denoted as #Z in the results section.

2.2. Conventional methanation

In conventional methanation, the reactor is filled with silicon carbide (CSi) and catalyst in a mass ratio of 4 to resemble the SEM arrangement. The gaseous feed stream is compressed just to overcome the pressure losses downstream. Depending on the configuration, a train composed of a heater, a fixed-bed reactor and a condenser is repeated a different number of times (Fig. 2) [51]. The target is to either reach a grid-quality SNG (95 vol% CH_4) or an industrial-grade SNG (99 vol% CH_4), while keeping at minimum the amount of catalyst used.

Different configurations are considered (see Table 1). Those

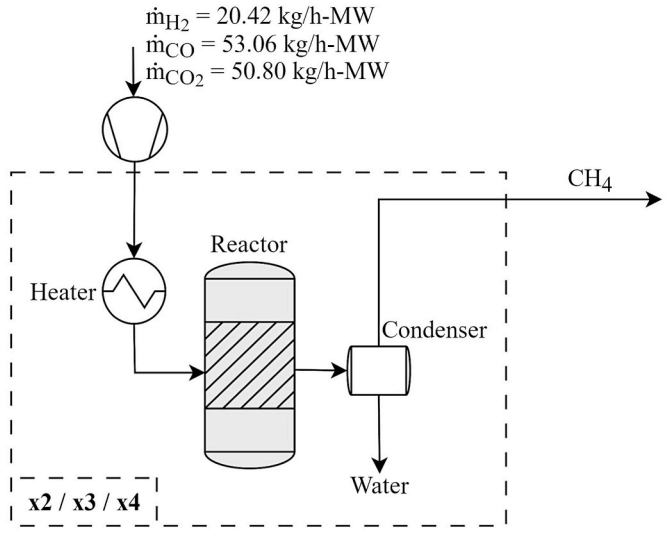

Fig. 2. Process flow diagram of a one-reactor conventional methanation system.

configurations aiming for 95 vol% CH_4 and operating at atmospheric pressure are labelled as #2, #3, #4, according to the number of reactors used. When technical constrains are applied, these cases are labelled as #2C, #3C and #4C. These constrains establish a maximum GHSV ($\leq$5000 h^{-1}) and a minimum temperature of operation ($\geq$300 °C), typical of industrial plants. Additionally, the #95P case operates at 10 bar, aiming to replicate the same conditions as those of the SEM case. Then, the configurations aiming for 99 vol% CH_4 are labelled as #99P and #99A. To that end, #99P uses a system pressure of 10 bar, whereas #99A operates at atmospheric pressure. In both cases, reactors are added in series until reaching 99 vol% CH_4 purity. The number of reactors is not known *a priori* for the #95P and the 99 vol% cases. The configuration with the fewest reactors that still achieves the desired purity is selected. The condenser temperature is assumed 35 °C in all cases (which is a conservative ambient temperature for most of the locations in the world), except for the #95P and the #99A case. These two exceptions respond to operational limitations and are explained more thoroughly in Section 4.2. For the #95P case, only a partial condensation occurs to adjust the final conversion to 95%. For the #99A case, a high reactor count is expected, so a sensitivity analysis is conducted regarding the effect of the condenser temperature and the number of reactors. In all cases, residual heats are integrated via a Pinch Analysis.

3. Methodology

3.1. Experimental setup

The performance of the SEM and the conventional methanation for the techno-economic assessment is supported on experimental data obtained at a lab-scale TRL-3 reactor (Fig. 3). In both cases, the same commercial Nickel-based catalyst is used, supplied by Haldor Topsoe [39,52]. For the SEM process, the chosen adsorbent is a commercial zeolite 4A supplied by Thermoscientific [38]. The TRL-3 reactor has been described in previous publications by the authors [39,40,53]. Briefly, the reactor consists of a stainless-steel vessel with an internal diameter of 1.8 cm and a hot zone height of 75 cm, externally heated by an electric wire. To accurately monitor the temperature profile during operation, a total of 14 thermocouples were placed along the bed (immersed 0.5 cm and spaced every 2.5 cm). A back-pressure valve downstream of the condenser allowed operation at pressures up to 10 bar, while two differential pressure sensors recorded the bed pressure drop. The feed gas composition (CO, CO_2, H_2 and N_2) was controlled using mass flow controllers. The gas mixture was preheated in a secondary furnace located upstream of the reactor to ensure complete vaporization and homogeneous inlet conditions. The outlet gas composition was analyzed continuously using a micro-chromatograph (Varian CP-4900), with a silica gel trap installed before the analyzer to ensure the efficient removal of water traces.

The fixed-bed configuration used for the SEM experiments consisted of 20 g of methanation catalyst physically mixed with 80 g of activated zeolite 4A, both with particle sizes in the range of 400–800 μm, yielding a packed bed height of 30 cm. For comparison, conventional methanation tests were performed under analogous conditions, replacing the zeolite with 80 g of SiC (VWR Chemicals BDH Prolabo, 200–300 μm) as an inert filler, resulting in a bed height of 20 cm. By knowing this physical distribution and the density of SiC (3210 kg/m^3), we can compute the density of the catalyst (770 kg/m^3) and the beds (1310 kg/m^3 for SEM bed and 1965 kg/m^3 for CM bed).

Firstly, a pre-reduction pretreatment procedure was applied to ensure reproducible operation (for both SEM and CM tests). This pre-reduction stage consisted of a heating period to 400 °C under a stream of 20/80 vol% H_2/N_2 in order to reduce the catalyst and/or simultaneously desorb any residual H_2O from the zeolite. The system was then cooled to the desired reaction temperature using the same gas mixture. Pretreatment was considered complete once no further H_2O was detected in the silica gel trap and no additional H_2 consumption was observed

Table 1
Parameters of the conventional methanation configurations. *To be optimized (see Section 4.2).

Configuration	#2	#3	#4	#2C	#3C	#4C	#95P	#99P	#99A
Electrolysis capacity (MW)	1.0	1.0	1.0	1.0	1.0	1.0	1.0	1.0	1.0
$\dot{m}_{H2}$ (kg/h)	20.4	20.4	20.4	20.4	20.4	20.4	20.4	20.4	20.4
$\dot{m}_{CO2}$ (kg/h)	50.3	50.3	50.3	50.3	50.3	50.3	50.3	50.3	50.3
$\dot{m}_{CO}$ (kg/h)	52.6	52.6	52.6	52.6	52.6	52.6	52.6	52.6	52.6
Pressure (atm)	1.0	1.0	1.0	1.0	1.0	1.0	10.0	10.0	1.0
Number of reactors	2	3	4	2	3	4	TBO*	TBO*	TBO*
Technical constrains									
GHSV (h^{-1})	-	-	-	≤5000	≤5000	≤5000	≤5000	≤5000	≤5000
T (°C)	-	-	-	≥300	≥300	≥300	≥300	≥300	≥300
CH_4 in SNG (vol% d.b.)	95.0	95.0	95.0	95.0	95.0	95.0	95.0	99.0	99.0
Condensers (°C)	35.0	35.0	35.0	35.0	35.0	35.0	TBO*	35.0	TBO*

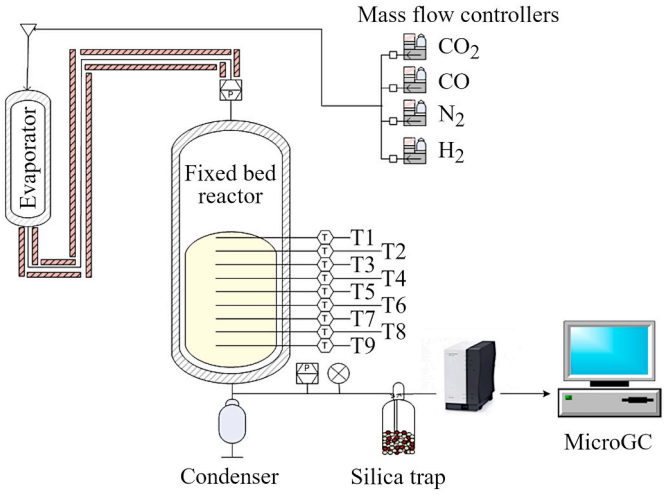

Fig. 3. Scheme of the TRL-3 fixed-bed reactor.

in the outlet gas.

The SEM and CM reaction were carried out using a feed consisting of a stoichiometric mixture of H_2, CO and CO_2 (i.e., M-module of 3, defined as $(H_2–CO_2)/(CO + CO_2)$). A small fraction of N_2 was also introduced as an internal standard. Conventional methanation experiments were performed starting at initial average solid temperatures between 189 °C and 268 °C, and pressures between 1 and 10 bar. During operation, the temperatures under steady state conditions reached 195 °C – 302 °C (hot spots could reach 420 °C). SEM experiments were conducted at an initial average solid temperature of 225 °C and a pressure of 10 bar (during operation, temperature remained below 280 °C). In conventional methanation, the space velocities were maintained between 0.5 and 1.2 $kg/kg_{cat}·h$ for both CO and CO_2 feeds. On the other side, the space velocities in SEM were maintained at 1 $kg_{CO}/kg_{cat}·h$ and 1 $kg_{CO2}/kg_{cat}·h$, in line with previously optimized conditions [39,40]. In all tests, the CO:CO_2 ratio is around 60:40 vol%, so the experimental conditions are representative of the scenarios of the techno-economic assessment.

To evaluate the performance of the catalyst, different indexes are used. Concretely, CO and CO_2 conversion (X_{CO} and X_{CO2}, Eq. (3) and Eq. (4)), and selectivity to CH_4 (S_{CH4}, Eq. (5)) [54], where $\dot{n}_i^{in}$ and $\dot{n}_i^{out}$ correspond to the inlet and outlet molar flow rates.

$$X_{CO_2} = \frac{\dot{n}_{H_2}^{in} - 3\dot{n}_{CO}^{in}X_{CO} - \dot{n}_{H_2}^{out}}{4\dot{n}_{CO_2}^{in}} \cdot 100 \tag{3}$$

$$X_{CO} = \frac{\dot{n}_{CO}^{in} - \dot{n}_{CO}^{out}}{\dot{n}_{CO}^{in}} \cdot 100 \tag{4}$$

$$S_{CH_4} = \frac{\dot{n}_{CH_4}^{out}}{\dot{n}_{CH_4}^{out} + \dot{n}_{CO}^{out}} \cdot 100 \tag{5}$$

3.2. Kinetic modelling

A kinetic model is adjusted to quantify the required amount of catalyst (and therefore the reactors' size) to be considered in the techno-economic assessment. The kinetic model is based on the reaction rates ($mol/g_{cat}·s$) proposed by Xu and Froment [55], following Eqs. (6) and (7) for RWGS and CO methanation, respectively:

$$r_1 = \frac{\frac{k_1}{p_{H_2}}\left(p_{CO}p_{H_2O} - \frac{p_{CO_2}p_{H_2}}{K_{eq1}}\right)}{\left(1 + K_{CO}p_{CO} + K_{H_2}p_{H_2} + K_{CH_4}p_{CH_4} + \frac{K_{H_2O}p_{H_2O}}{p_{H_2}}\right)^2} \tag{6}$$

$$r_2 = \frac{\frac{k_2}{p_{H_2}^{2.5}}\left(p_{CH_4}p_{H_2O} - \frac{p_{CO}p_{H_2}^3}{K_{eq2}}\right)}{\left(1 + K_{CO}p_{CO} + K_{H_2}p_{H_2} + K_{CH_4}p_{CH_4} + \frac{K_{H_2O}p_{H_2O}}{p_{H_2}}\right)^2} \tag{7}$$

where p_i are the partial pressures (Pa) of the components, k_j (Eq. (8)) and K_{eq} (Eqs. (9) and (10)) are the rate coefficient ($mol/(g_{cat}·s·Pa)$ for k_1 and $mol·Pa^{0.5}/(g_{cat}·s)$ for k_2) and the equilibrium constant (unitless for K_{eq1} and Pa^2 for K_{eq2}) of each reaction, and K_i are the adsorption constants (1/Pa for CO, CH_4, H_2, unitless for H_2O) of each component (Eq. (11)).

$$k_j = k_{j,0}·\exp\left(-\frac{E_{A,j}}{R·T}\right) \tag{8}$$

$$K_{eq1} = \exp\left(\frac{4400}{T} - 4.063\right) \tag{9}$$

$$K_{eq2} = 1.026676 \times 10^{10} \exp\left(\frac{-26830}{T} + 30.11\right) \tag{10}$$

$$K_i = K_{i,0}·\exp\left(-\frac{\Delta H_i^0}{R·T}\right) \tag{11}$$

The parameters $k_{j,0}$ (pre-exponential factor, same units as k_1 and k_2), $E_{A,j}$ (activation energy, J/mol), $K_{i,0}$ (adsorption constants, same as for K_i), and ΔH_i^0 (enthalpies of adsorption, J/mol) were obtained by minimizing the arithmetic mean (Eq. (12)) of the mean squared error (MSE) for the volumetric concentration of each component in the outlet gas (Eq. (13)). The volumetric concentration of each component is defined according to Eq. (14), where $\dot{n}_i^{out}$ is the mole flow of component i at the outlet. The M_{MSE} was minimized by using the Powell Method [56].

$$M_{MSE} = \frac{\sum_i MSE_i}{N_i} \tag{12}$$

$$MSE_i = \sqrt{\frac{\sum_j \left(x_{ij}^{model} - x_{ij}^{test}\right)^2}{N_j}} \quad (13)$$

$$x_i = \frac{\dot{n}_i^{out}}{\sum_i \dot{n}_i^{out}} \cdot 100 \quad (14)$$

This methodology was applied for the conventional methanation (9 tests were used to adjust the parameters, and 7 tests to validate the model). This cannot be applied to sorption-enhanced methanation, since CO_2 and CO conversion is 100% at all conditions. More details can be found in section 4.1.

3.3. Technical assessment

The technical assessment of SEM and CM is performed through Aspen Plus simulation, assuming the inlet flows described in Section 2. For the sorption-enhanced methanation (Case #Z), the methanators are modelled as stoichiometric reactors (RStoic) with 100% conversion. The required amount of catalyst is calculated by assuming the same $WHSV_{H2}$ than in the experimental tests (i.e., 0.12 kg_{H2}/kg_{cat}·h). For conventional methanation, the methanators are modelled as plug reactors (RPlug), which include the implementation of the reaction kinetics. The amount of catalyst needed in each case for CM is minimized by using the optimization tool of Aspen Plus, applying technical constraints if the case requires it (see constrains in Table 1).

The compressor work, the heating and the cooling needs are extracted from Aspen Plus. For the compressor work, it is a straightforward process. Conversely, the heat integration of preheaters and reactor cooling is studied with a Pinch analysis, which is detailed in the results section. Cooling water at 25 °C is considered as the cold utility, whereas electricity is considered as the hot utility (assuming 1 MJ electricity = 1 MJ heat for the sake of simplicity). The goal of the analysis was to assess how much external electricity is required to complete the heat integration. The pinch point temperature is assumed to be 10 °C.

For most of the cases, no refrigeration work is required as the condenser operates at 35 °C. Nonetheless, it will be explained that the #99A requires condensation at 0 °C. The calculation of the refrigeration electrical work is obtained by dividing the thermal refrigeration needs by the ideal efficiency of a refrigeration Carnot cycle, in which the hot reservoir is at ambient temperature (25 °C), and the cold reservoir is at 0 °C (COP = 10.92).

3.4. Economic assessment

The economic study was assumed to be a retrofit of an existing industrial plant who desired to abate their emissions, revalorizing them. The cost equations for the different elements of the economic analysis are summarized in Table S1 (supplementary material). These include the correlations used to calculate the CAPEX, the OPEX and the INCOMES.

The capital expenditure (CAPEX) is divided into process direct costs, other direct costs, and indirect costs. The process direct costs are the methanation reactors, compressors, exchangers, the catalyst and the filler (CSi in the CM cases and zeolite in SEM). The cost of catalyst, zeolite and CSi is 93750 €/t [57], 408 €/t [58] and 305 €/t [59], respectively. The equation cost for the first methanation reactor varies whether it is a restricted case or not. This is depicted in Fig. 4. For the restricted case, a specific price of 300 €/kW is considered [60]. This price assumes a fixed bed reactor with a size smaller than 10 MW, as well as the technical limitations of an industrial plant, such as the GHSV limitations explained before. Additionally, the effect of the operating pressure is considered [61]. Nevertheless, the unrestricted reactors are smaller, and consequently cheaper. Therefore, their cost scales as a function of the reactor size and the price of the restricted case (#3C considered as benchmark). Regarding the cost of subsequent reactors, the same procedure for each case is followed (see Fig. 4), scaling it as a function of the size of the first reactor of each case. A typical scale factor of 0.65 is considered.

The direct costs have been also adjusted by the CEPCI index when required, according to the publication year of each reference. Other direct costs include installation, instrumentation, control, piping, electrical elements and the building itself. Indirect costs include engineering, legal expenses, construction expenses, and a reserve for contingencies. All of them are computed as a percentage of the total Process direct cost.

The operational expenditure (OPEX) includes the consumption of hydrogen and electricity as well as the yearly renovation of 15% of the catalyst and fillers. The cost of hydrogen is assumed to be 6 €/kg, according to estimations of the IEA for electrolytic hydrogen for 2030, considering the net zero scenario for 2050 (2-7 USD/kg_{H2} when using electricity from onshore wind farms, and 2-5 USD/kg_{H2} from photovoltaic plants) [62]. Electricity price is taken from the Spanish market for April 2025 (66 €/MWh) [63]. Nitrogen price is not necessary, as it is only used in #Z and operates in a closed loop.

In terms of incomes, there are two items. Firstly, the carbon entering methanation is considered abated, as described in Eq. (15). Therefore, the CO_2 tax of those emissions can be considered as income (savings).

$$\dot{m}_{CO_2,abated} = \dot{m}_{CO_2} + \frac{44}{28}\dot{m}_{CO} \quad (15)$$

Secondly, the SNG obtained is sold. Depending on the purity of the SNG produced, the price changes. For the 95% CH_4 cases (#2, #3, #4, #2C, #3C, #4C and #95P), price is taken from the Spanish natural gas market for April 2025 (35 €/MWh, or 0.49 €/kg) [64]. Price for the 99%

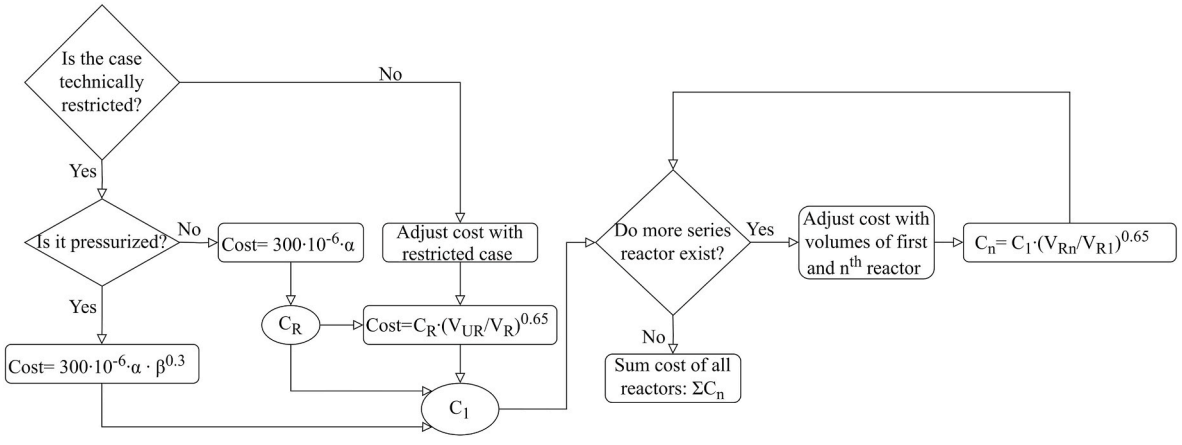

Fig. 4. Flowchart for reactor cost calculation (see details in Table S1).

CH_4 cases (#99P, #99A) is considered 4.2 €/kg [65].

For the zeolite case (#Z), whose purity is 100%, a price for a 99.9% CH_4 gas is assumed (12 €/kg) [66]. Other additional costs that may appear for such high purities, like post-processing purification, compression, quality control, packaging and logistics, were considered out-of-scope. This is addressed again in the results section.

3.5. Key performance indicators

Different key performance indicators are defined to quantify the techno-economic analysis (Table 2). The technical KPIs are classified into reactor-specific and global, and they are reported per unit of MW_e provided as input to the electrolyser. The economic KPIs are reported for a plant size of 200 MW_e in line with some of the major ongoing projects, such as the plant commissioned in Kristinestad, Finland [67].

Reactor-specific KPIs are related to conventional methanation only, and they are used to characterize each of the reactors of the methanation plant. These include both operating parameters (temperature, GHSV, outlet CH_4 fraction, and cooling necessities) and sizing parameters (catalyst mass, filler mass and reactor's volume). The GHSV is calculated with the volumetric flow rate of reactants F at STP conditions.

Global KPIs characterize the entire methanation plant. They quantify the total thermal and electrical necessities, in addition to the total catalyst mass and reactors' volume. It must be noted that most of the thermal energy required to preheat the inlet gas of the reactors is covered by heat integration (since reactors and condensers have cooling requirements). The rest is supplied by electric heating (a 100% electricity-to-heat efficiency is considered). Moreover, case #99A requires electric power for refrigeration, as condensers operate at 0 °C. Therefore, the total electricity consumption is the sum of the electric heating, refrigeration, and compressors' work.

Economic KPIs include the CAPEX, OPEX, yearly incomes, the specific implementation cost (SIC) and the levelized cost of methane (LCOM). The SIC is calculated as the quotient of the net present value (NPV) after 20 years of operation and the total SNG produced in the same time span. When it is negative, it represents profitability (NPV >0), when it is positive, the opposite (NPV <0). Meanwhile, LCOM represents the selling price that would be sufficient to provide profitability (SIC = 0 or NPV = 0). An annual interest of 4% is considered when computing the NPV.

Table 2
Key performance indicators.

KPI	Units	Calculated as
Reactor-specific		
T (°C)	°C	Aspen Plus optimization
GHSV	h^{-1}	$F/(m_{cat}/\rho_{cat})$
CH_4 in outlet gas	vol% db	$x_{CH4}/(100 - x_{H2O})$
Cooling (reactor)	kW/MW_e	Aspen Plus optimization
m_{cat}	kg/MW_e	Aspen Plus optimization
M_{CSi}	kg/MW_e	m_{cat}·4
Volume	l/MW_e	$1000\cdot(m_{cat} + m_{alum})/\rho_{bed}$
Global		
Heating (covered by heat integration)	kW/MW_e	$\sum q_{heater,i}$
Cooling (reactors)	kW/MW_e	$\sum q_{reac,i}$
Cooling (condensers)	kW/MW_e	$\sum q_{cond,i}$
Electricity consumption	kW/MW_e	$w_{heater} + \sum q_{cond,0^\circ C,i}/COP_{carnot} + w_{comp}$
Electric heating	kW/MW_e	Pinch Analysis
Refrigeration	kW/MW_e	$\sum q_{cond,0^\circ C,i}/COP_{carnot}$
Compressor work	kW/MW_e	Aspen Plus optimization
m_{cat}	kg/MW_e	$\sum m_{cat,i}$
Volume	l/MW_e	$\sum v_i$
Economic		
CAPEX	M€	$C_{reactor} + C_{equip} + C_{mat,filler} + C_{direct} + C_{indirect}$
OPEX	M€/y	$O_{H2} + O_{Elec} + O_{N2} + O_{cat,\ filler} + O_{O\&M}$
Yearly incomes	M€/y	$I_{CO2} + I_{SNG}$
SIC (20 years)	€/kg_{SNG}	$-10^3\cdot NPV/m_{SNG,20\ years}$
LCOM	€/kg_{SNG}	Selling price of SNG so NPV = 0

4. Results and discussion

4.1. Experimental tests and kinetics

4.1.1. Conventional methanation

Several experiments were conducted under different operating conditions for the conventional methanation process to generate a dataset for model development and validation (kinetic model is used to quantify the catalyst needed and the reactors' size, during the techno-economic assessment). Nine experiments were selected for kinetic fitting and seven for validation. The feed composition remained nearly constant in all tests (i.e. 77 vol% H_2, 14–15 vol% CO, and 8–10 vol% CO_2), with a total flow of 67 l/h (STP). Pressure, temperature, and gas space velocity were varied across the campaign. All the results are summarized in Table 3, which correspond to the steady-state regime, once bed temperature and outlet composition were stable (detailed data can be found in the supplementary material, in Table S2).

As shown in Table 3, the performance of CM reactor was consistently

Table 3
Experimental data obtained for conventional methanation at TRL-3.

Experiment	#1	#2	#3	#4	#5	#6	#7	#8	#9	#10	#11	#12	#13	#14	#15	#16
Fitting/Validation	Fitt.	Fitt.	Fitt.	Fitt.	Val.	Val.	Val.	Fitt.	Fitt.	Fitt.	Val.	Val.	Fitt.	Val.	Fitt.	Val.
P (bar)	1	5	5	5	10	10	10	10	10	10	10	10	10	10	10	10
GHSV (h^{-1})	2568	3982	3848	2568	3993	3993	4080	5201	4080	4080	4080	4080	2568	2465	2568	2568
WHSV ($kg_{CO}/(kg_{Cat}\cdot h)$)	0.6	1.0	0.8	0.6	0.9	0.9	0.9	1.2	0.9	0.9	0.9	0.9	0.6	0.6	0.6	0.6
WHSV ($kg_{CO2}/(kg_{Cat}\cdot h)$)	0.6	0.8	1.0	0.6	0.9	0.9	0.9	1.1	0.9	0.9	0.9	0.9	0.6	0.5	0.6	0.6
T (°C) initial average solid temperature	240	242	268	245	189	189	202	241	208	252	221	243	224	246	258	242
Product gas composition (vol%)																
H_2	6.9	67.9	1.7	2.9	70.9	73.3	2.6	2.6	2.0	1.9	1.8	2.1	2.1	1.7	2.4	1.9
CO	0	16.5	0	0	11.5	10.9	0	0	0	0	0	0	0	0	0	0
CO_2	2.5	8.2	5.0	1.4	9.8	9.1	2.9	2.6	2.5	1.9	1.8	1.7	1.5	1.3	1.1	0.6
CH_4	36.2	2.9	37.3	38.2	3.1	2.7	37.8	37.9	38.2	38.5	38.6	38.5	38.6	38.9	38.6	39.0
H_2O	54.4	4.3	55.9	57.4	4.7	4.1	56.6	56.9	57.4	57.7	57.8	57.7	57.8	58.3	57.8	58.4
Performance (%)																
X_{CO}	100.0	15.6	100.0	100.0	27.2	26.8	100.0	100.0	100.0	100.0	100.0	100.0	100.0	100.0	100.0	100.0
X_{CO2}	84.4	21.1	73.2	91.3	0	0	82.0	83.2	84.5	88.1	88.7	89.3	91.0	91.0	93.1	95.9
S_{CH4}	100.0	18.0	100.0	100.0	25.3	23.8	100.0	100.0	100.0	100.0	100.0	100.0	100.0	100.0	100.0	100.0

Table 4
Adjusted values for the parameters of the kinetic model for the experiments on conventional methanation of this study.

Parameter	Units	This study	Xu & Froment
$E_{A,1}$	J/mol	70382	67130
$E_{A,2}$	J/mol	238479	240100
$k_{1,0}$	mol/(g_{cat} s Pa)	63334	$5.42{\cdot}10^{-3}$
$k_{2,0}$	mol $Pa^{0.5}$/(g_{cat} s)	$3.299{\cdot}10^{15}$	$3.69{\cdot}10^{14}$
$K_{CO,0}$	1/Pa	$1.126{\cdot}10^{-16}$	$8.23{\cdot}10^{-10}$
$K_{H2,0}$	1/Pa	$1.628{\cdot}10^{-23}$	$6.12{\cdot}10^{-14}$
$K_{CH4,0}$	1/Pa	$1.085{\cdot}10^{-10}$	$6.65{\cdot}10^{-9}$
$K_{H2O,0}$	-	6.9	$1.77{\cdot}10^{5}$
ΔH^0_{CO}	J/mol	− 141503	− 70650
ΔH^0_{H2}	J/mol	− 80650	− 82900
ΔH^0_{CH4}	J/mol	− 47735	− 38280
ΔH^0_{H2O}	J/mol	569705	88680

high for the experiments performed at pressures between 5 and 10 bar and average steady-state bed temperatures above 250 °C. In all these cases, X_{CO} was complete, while X_{CO2} ranged from 73.2% to 95.9%. When comparing experiments at different space velocities, a clear trend was observed: the highest X_{CO2} (>90%) occurred under the lowest GHSV values (~2500 h^{-1} or ~0.6 $kg_{COx}/h{\cdot}kg_{cat}$), where the longer residence time allowed the system to approach thermodynamic equilibrium more closely. These tests typically reached in steady stage an average solid bed temperature between 257 and 290 °C, confirming that both temperature and contact time strongly influence CO_2 methanation, in agreement with the intrinsic kinetics reported for Ni-based catalysts. Under these optimal conditions, the product gas composition was dominated by 38–40 vol% CH_4 and 56–58 vol% H_2O, with only trace amounts of CO_2 and H_2 (<2 vol%). This contrasts sharply with the behavior observed in the experiments performed at the lowest initial bed temperatures (189 °C), where the reactor stabilized at ≈195–205 °C and conversions were significantly limited (X_{CO} ≈ 26% and X_{CO2} ≈ 0%). In these low-temperature tests, the product stream consisted predominantly of unreacted H_2 (71–73 vol%), with 10 vol% CO_2, 10–11 vol% CO, and only 3–4 vol% CH_4, demonstrating that insufficient thermal activation severely restricts the activity of the Ni catalyst even at 10 bar.

A second deviation from the high-performance region was found in the experiment conducted at the highest space velocity (3982 h^{-1}) within the moderate pressure (5 bar), where residence time became the limiting factor. Despite reaching a steady-state average temperature of 245 °C, higher than the low-temperature cases mentioned above, the conversions remained modest (X_{CO}:15.6% and X_{CO2}: 21.1%). Comparatively, experiments carried out at similar pressures and initial average bed temperature but lower GHSV consistently showed much higher X_{CO} and X_{CO2}, confirming that space velocity exerts a stronger influence at intermediate temperatures, where kinetic limitations become more pronounced.

Overall, by contrasting the three characteristic operating regimes (i) low temperature, (ii) intermediate temperature but high GHSV, and (iii) optimal temperature with moderate-to-low GHSV, the dataset clearly demonstrates that temperature and residence time act synergistically, defining the transition between kinetically limited and equilibrium-approaching operation. This behavior is fully consistent with the bifunctional nature of the methanation network: while CO methanation reaches equilibrium rapidly under all conditions with sufficient temperature, CO_2 methanation remains more sensitive to both temperature and contact time, requiring temperatures in the steady stage above 250 °C and reduced GHSV to attain conversions above 90%.

Nine of these experimental tests were used to fit the parameters of the kinetic model that are shown in Table 4; the rest were used to validate the model. The simulated model showed an agreement with the experimental data within ±10% error (Fig. 5), when reproducing the outlet gas volumetric concentrations under the different operating conditions. The kinetic model will be used to size the reactors of the methanation plant for the techno-economic analysis.

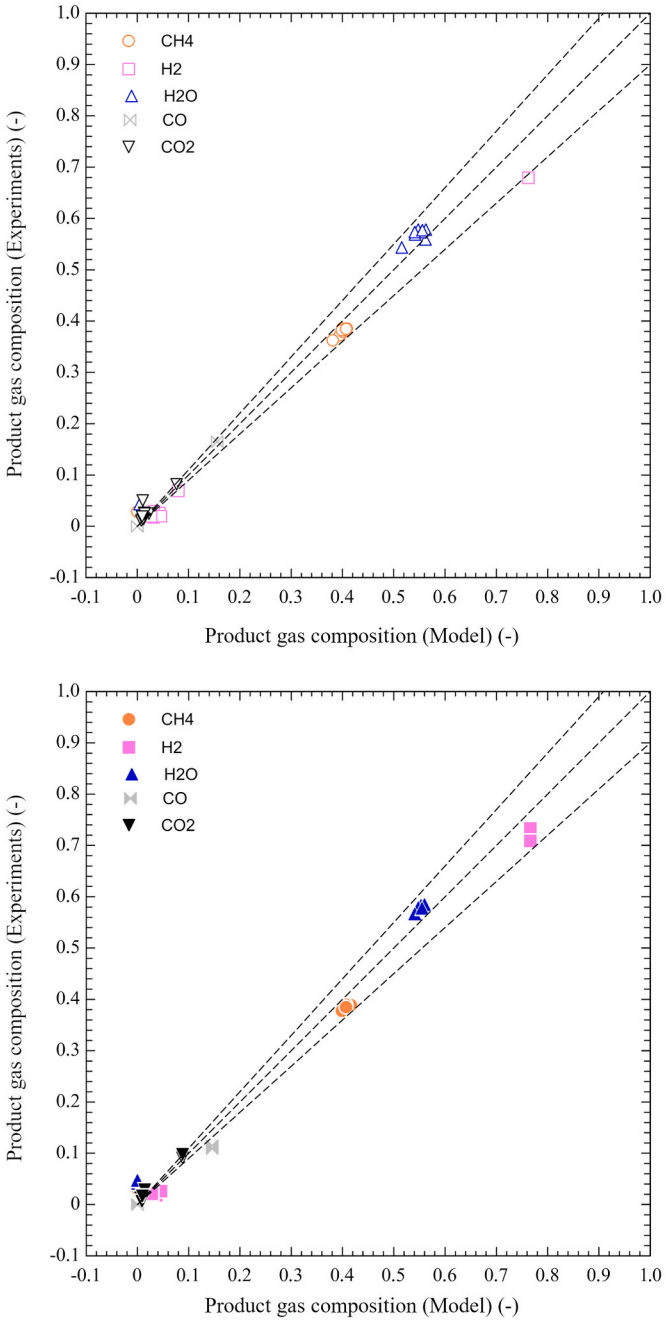

Fig. 5. Parity plot of product gas composition for conventional methanation tests. Up: model fitting; Down: model validation. Dashed lines represent ±10% error.

4.1.2. *Sorption-enhanced methanation*

As noticed from the experimental results shown in (Table 3), the maximum purity of CH_4 reached under CM conditions was approximately 39 vol% (93.9 vol% d.b.), obtained from nearly complete CO and CO_2 conversions at initial average solid temperatures around 242 °C (achieving an average of 279 °C under steady stage conditions) and high pressures, under low gas space velocity conditions. This result is consistent with thermodynamic predictions, which suggest an upper limit of around 95.8 vol% d.b. of CH_4 under these conditions (10 bar and 250 °C). Contrarily, SEM conditions resulted in CH_4 purity of up to 100 vol%, due to the in-situ adsorption of H_2O by the zeolite [28,39]. The

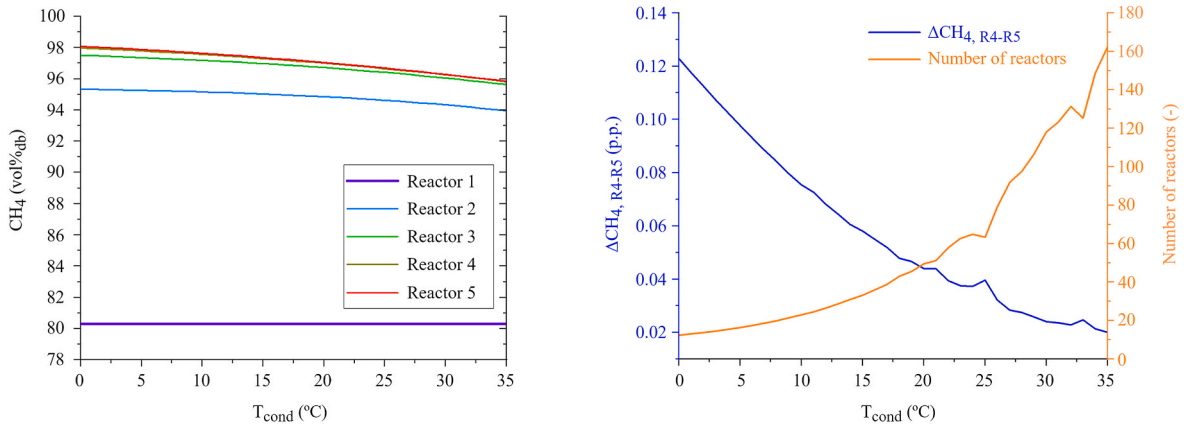

Fig. 6. Left: CH_4 vol% d.b. Reached at each reactor outlet vs. condenser temperature under CM conditions; Right: Variation in CH_4 vol% d.b. in percentual points between reactor 4 and 5 ($\Delta CH_{4,R4-R5}$) vs. condenser temperature, and total amount of reactors required to reach 99%$_{dry}$ CH_4 considering $\Delta CH_{4,R4-R5}$ constant.

experimental methodology used for SEM was similar to that used for CM, but the presence of a zeolite in the solid bed, which has a finite adsorption capacity of H_2O, led to the existence of an unsteady state profile at the outlet of the reactor. The most relevant period corresponds to the pre-breakthrough period, during which the zeolite effectively adsorbs the H_2O generated by the reaction, thereby enhancing CH_4 purity. Once the zeolite is saturated, H_2O begins to appear in the product stream, transitioning the process to the post-breakthrough period where CM is fulfilled and CH_4 purity declines [28,39].

For this study, a representative SEM experiment was performed at 10 bar, with a WHSV of 1 $kg_{CO}/h{\cdot}kg_{cat}$ and 1 $kg_{CO2}/h{\cdot}kg_{cat}$ (i.e., 4424 h^{-1} GHSV), and an initial average solid bed temperature of 225 °C. The feed gas consisted of $H_2/CO/CO_2$ in stoichiometric proportions (M-module equal to 3). Under these operating conditions, the zeolite adsorbed H_2O for around 15 min, corresponding to an H_2O uptake capacity of 12.2 $g_{H2O}/g_{zeolite}{\cdot}100$. During this period, complete conversion of CO, CO_2 and H_2 was achieved, producing 100% purity CH_4 and a productivity of 0.016 $mol_{CH4}/kg_{cat}{\cdot}s$. After this pre-breakthrough stage, the pressure was reduced to atmospheric conditions and 300 l/h (STP) of a 90 + 10 vol% N_2+H_2 gas mixture was fed for 45 min while maintaining the same reaction temperature, in order to carry out a regeneration step [68]. The suitability of these conditions during SEM and regeneration has been demonstrated along multiple cycles in earlier studies [39,40].

4.2. Aspen Plus simulation

4.2.1. Reactor optimization

Each process was simulated in Aspen Plus v.11. The SEM case was straightforward, as it mimicked the configuration presented in Fig. 1. Therefore, the reactions were simulated by stoichiometric reactors with 100% conversion, and the main goal was to study the electricity consumption and thermal needs of the system. The heat required for the N_2/H_2 regeneration flow was calculated using a simple heat exchanger model. For the conventional methanation cases, an optimization effort was required to provide the best process configurations for the proposed case studies. The aim was reaching a certain CH_4 vol% fraction in the SNG, while keeping the required mass of catalyst at minimum in favor of profitability. However, this led to discard some of the cases. For example, there was no scenario in which #2C reached a 95 vol% CH_4 composition while in compliance with the technical constraints. On the other hand, #4C was unnecessary, as the minimum GHSV constraint guarantees a CH_4 concentration at the exit of the third reactor that is always over 95 vol%. Therefore, the #4C results are identical to #3C, with the addition of a fourth reactor that would only worse economic results. The number of reactors for the #95P case was left as a design variable, requiring only two reactors to reach the desired 95 vol% CH_4 purity. Nonetheless, it presented some additional challenges. The technical limitations rendered results that were always below 95 vol% CH_4 purity for the first reactor, and over 95 vol% CH_4 purity for the second reactor. The first idea to solve that was to increase the temperature of the second reactor, limiting the reaction from a thermodynamic point of view. Nonetheless, it does not make sense to spend more energy to preheat the reactor to obtain a lesser energy output. Therefore, it was decided to increase the condensation temperature between both reactors, reducing the energy consumption. With this configuration, the stream is cooled to only 139 °C between reactors.

Regarding cases aiming for 99 vol% CH_4, the number of reactors was also a design variable, like in the #95P case. For the #99P case operating at 10 atm, 3 reactors were sufficient to reach the required purity. For the atmospheric pressure case #99A, a really high number of reactors would be required if condensers operate at 35 °C as usual. Therefore, a sensitivity analysis was conducted, in which the condenser temperature was varied down to 0 °C (Fig. 6). The left part of the graph shows the CH_4 dry volumetric fraction at the outlet of the first five reactors, as a function of the condenser temperature. Based on the sensitivity analysis shown in this figure, a purity of 99 vol% CH_4 is not possible regardless of the condenser temperature for the first five reactors. The difference in concentration between the fourth and the fifth reactor, in percentual points, was labelled as $\Delta CH_{4,\ R4-R5}$, and it is represented in Fig. 6 right as a function of condenser temperature. Considering this parameter as constant for the following reactors, the amount number of required series reactor to reach 99 vol% CH_4 was calculated. Over 160 reactors would be required with a condenser temperature of 35 °C, and only 13 reactors would be needed if the condenser temperature is 0 °C. Thus, for the #99A case, it was considered that condensers operate at 0 °C.

To wrap up the optimization of conventional methanation, the operating diagrams of all cases are depicted in Fig. 7 (95 vol% purity cases) and Fig. 8 (99 vol% purity cases). These diagrams show the evolution of the CH_4 composition on a dry basis after each methanation stage (solid line). The diagonal segments represent a heater + reactor stage, while the vertical ones represent the cooling by the condensers. Meanwhile, the dashed lines represent the equilibrium curves of the different reactors. These curves differ for each reactor since water is condensed between stages. It can be seen in Fig. 7 that the reactors of non-restricted cases are more evenly spaced, whereas the thermodynamic states of #3C, and specially #95P, are shifted to the right. This is more notorious for the 99% cases (Fig. 8). For the #99P case, the first reactor already reaches over 90% CH_4 (like #95P). For the #99A case, conversion after the third reactor is residual.

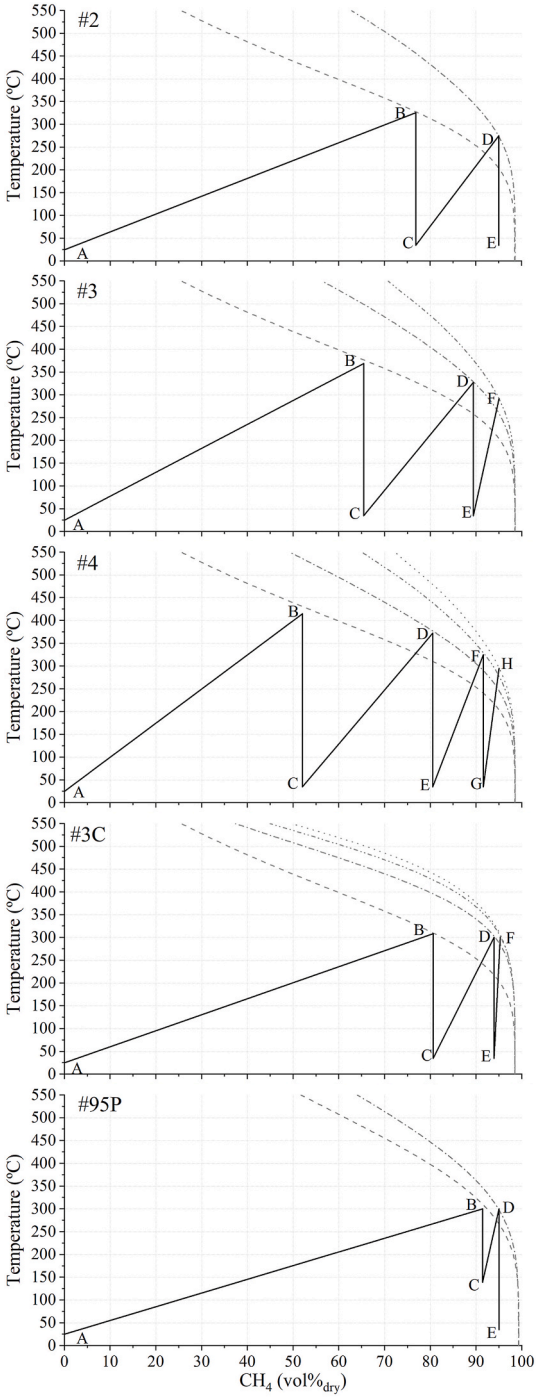

Fig. 7. Operating diagrams (95 vol% CH_4 cases).

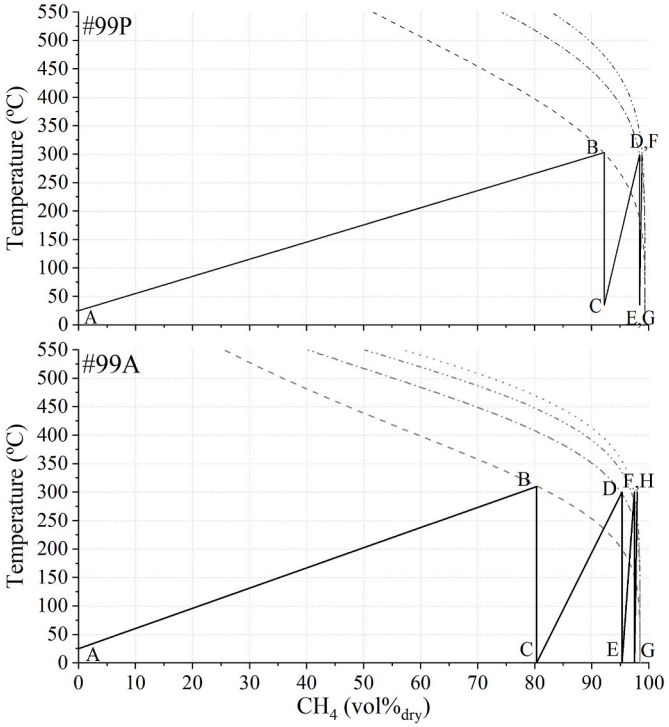

Fig. 8. Operating diagrams (99 vol% CH_4 cases).

4.2.2. Pinch analysis

Regarding heat integration, it was designed aiming at minimizing the need for electric heating in all scenarios. For the zeolite SEM case, the available heat from the reactors (175 kW/MW_e) exceeds the N_2+H_2 preheat requirements (3.4 kW/MW_e). Moreover, as the reactor temperature is also higher than the required preheat temperature, it is assumed that the reactor can fulfil all its preheating requirements. The H_2/CO/CO_2 flow is heated thanks to its compression to 10 bar up to 200 °C, which is fixed as the technical operation limit of the compressor. The remaining 40 °C are provided by electricity (4.56 kW/MW_e)

In the case of conventional methanation, the Pinch analysis method was used for designing the heat integration. As the process is similar for all the configurations, Case #2 was used as an illustrative example. Fig. 9 shows the optimal heat exchanger network for this case. The cold utility (cooling water) and the heat sink streams are depicted in blue, whereas the hot utility (electricity) and the heat source streams are depicted in red (R1 and R2 indicate the heat evacuated from first and second reactors, whereas C1 and C2 refer to the cooling stages placed at the outlet of reactor 1 and 2 respectively). Therefore, the red heat exchanger represents the external electricity requirements. The electricity required for the cooling water is not considered into the analysis, as it operates at ambient temperature. This is not the case for #99A, where a refrigerant-based cold utility is added into the analysis. The results of each Pinch analysis are presented as KPIs, within the electricity consumption.

4.3. Technical KPIs

4.3.1. Reactor-specific (conventional methanation)

In this section, technical KPIs are compared between the different CM case studies from a reactor-specific perspective. When paying attention to reactor-specific KPIs, two different patterns can be observed, depending on whether there are technical constraints or not. For the cases #2, #3 and #4, the catalyst mass is at its lowest in the first reactor and then greater in the followings (Table 5). Looking at the CH_4 concentrations at the outlet, the optimal way of decreasing the mass catalyst is to present moderate, similar conversions in each reactor. These cases, specially the #4 case, feature really high GHSVs, which are not feasible in practice. Conversely, for the rest of the cases, the catalyst mass tends to decrease with the following reactors (#3C, #95P, #99P and #99A). Most of the conversion is reached within the first reactor, and the rest of them are simply set to the minimum temperature (300 °C) and the maximum GHSV (5000 h^{-1}) available (Fig. 10). As a final comment, only the first 4 reactors are included for the #99A case in Table 5. Fifth and onwards reactors are considered to be identical to the fourth reactor, and to present a constant $\Delta CH_{4,R4–R5}$.

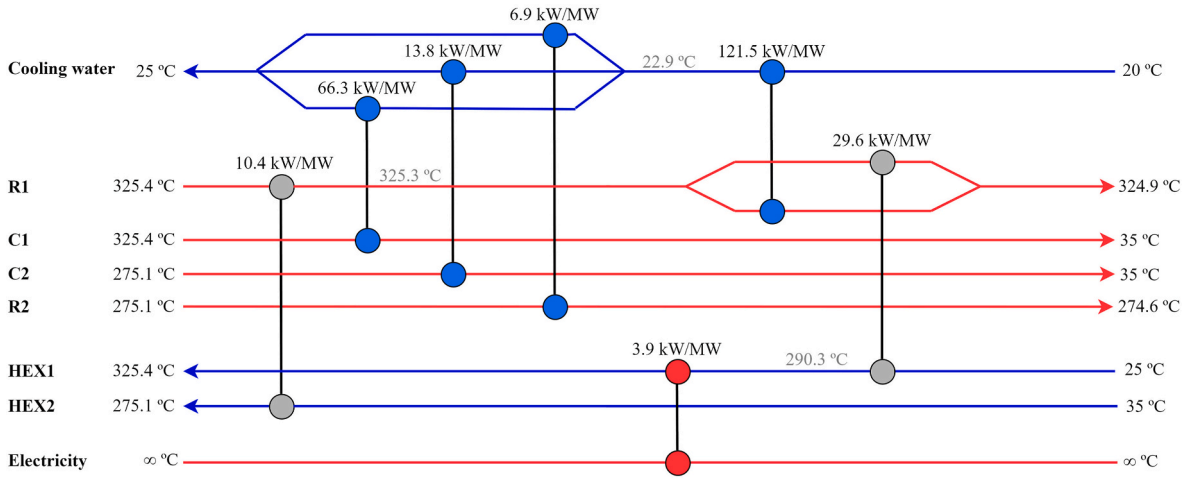

Fig. 9. Optimal network resulting from the Pinch analysis for CM case #2.

Table 5
Comparison of reactor-specific technical KPIs for CM scenarios.

Configuration	#2	#3	#4	#3C	#95P	#99P	#99A
Reactor 1							
T (°C)	325.4	368.7	414.8	308.4	300.0	303.3	310.2
GHSV (h^{-1})	10412	55000	239960	5000	5000	5000	5000
CH_4 in outlet gas (vol% d.b.)	77.0	65.4	52.0	80.6	91.4	92.2	80.3
Cooling (reactor) (kW/MW_e)	161.5	156.6	148.0	162.7	166.3	166.7	162.0
m_{cat} (kg/MW_e)	24.4	4.6	1.1	50.8	50.7	50.7	50.7
m_{fill} (kg/MW_e)	97.6	18.5	4.2	203.1	202.6	202.6	202.8
Volume (l/MW_e)	61.0	11.5	2.6	126.9	126.7	126.7	126.8
Reactor 2							
T (°C)	275.1	327.3	372.0	300.0	300.0	300.0	300.0
GHSV (h^{-1})	1679	15646	71865	5000	5000	5000	5000
CH_4 in outlet gas (vol% d.b.)	95.0	89.4	80.5	93.9	95.0	98.4	95.3
Cooling (reactor) (kW/MW_e)	6.89	10.9	16.92	4.91	1.19	1.97	5.48
m_{cat} (kg/MW_e)	45.0	5.43	1.4	14.6	19.73	12.4	13.8
m_{fill} (kg/MW_e)	180.0	21.7	5.6	58.2	78.91	49.5	55.3
Volume (l/MW_e)	112.5	13.6	3.5	36.4	49.3	30.9	34.6
Reactor 3							
T (°C)	-	291.3	324.5	300.0	-	300.0	300.0
GHSV (h^{-1})	-	6523	22854	5000	-	5000	30.3
CH_4 in outlet gas (vol% d.b.)	-	95.0	91.6	95.3	-	99.0	97.5
Cooling (reactor) (kW/MW_e)	-	1.9	4.28	4.28	-	0.13	0.67
m_{cat} (kg/MW_e)	-	10.3	3.2	12.9	-	11.8	12.1
m_{fill} (kg/MW_e)	-	41.2	12.8	51.7	-	47.0	48.4
Volume (l/MW_e)	-	25.8	8.0	32.3	-	29.4	30.3
Reactor 4							
T (°C)	-	-	294.6	-	-	-	300.0
GHSV (h^{-1})	-	-	9800	-	-	-	5000
CH_4 in outlet gas (vol% d.b.)	-	-	95.0	-	-	-	98.0
Cooling (kW/MW_e)	-	-	1.2	-	-	-	0.1
m_{cat} (kg/MW_e)	-	-	6.73	-	-	-	11.9
m_{fill} (kg/MW_e)	-	-	26.92	-	-	-	47.6
Volume (l/MW_e)	-	-	16.83	-	-	-	29.7

4.3.2. Global

In this section, technical KPIs are compared between the different case studies from a global perspective (Table 6). First, heat integration by Pinch analysis shows that 90% to 98% of preheating requirements are covered in CM, and 84% in SEM (Case #Z). The rest of the preheating requirements must be provided by electric heating, which in the worst case may represent up to 36% of the total electricity consumption (Case #2). This is driven by the higher simplicity of the design, that leaves less room for heat integration. In other words, in cases with a higher number of reactors there is a higher number of theoretical heat integrations, allowing for more efficient ones. This is sufficient to offset the increase of the heating needs of those cases.

The total cooling demand for reactors is similar in all cases, as this is related to the heat released during methanation (around 170 kW/MW_e). However, the cooling requirement for condensers is dependent on the number of reactors and operating conditions. Firstly, the condenser in the zeolite SEM case presents the lowest cooling requirement. Regarding the CM cases, Case #99A, for which there are 13 stages with condensers at 0 °C, needs almost double the cooling than for the other configurations (which on top of that must be fulfilled with electricity as it is below ambient temperature). The lowest cooling requirement of the CM cases is #95P case, due to the different condensation strategy.

Regarding electricity, the compressor is the main consumer of the plant (except for case #99A, in which electric heating and refrigeration accounts for 84% of the electricity consumption). The main driver for compressors' work is the operating pressure. Cases at ambient pressure

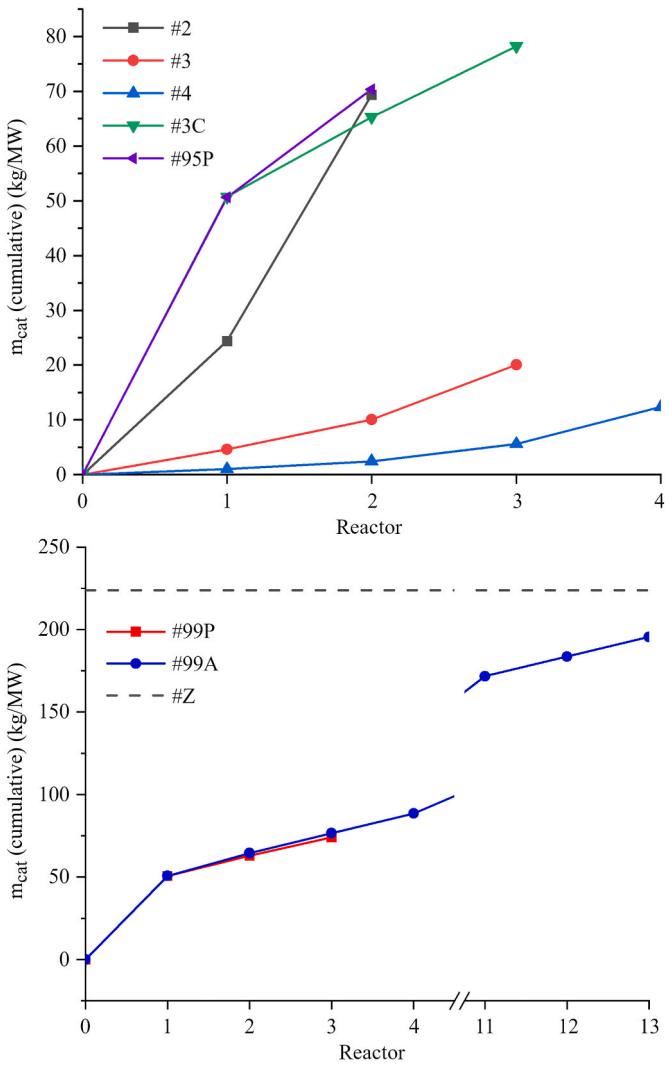

Fig. 10. Cumulative catalyst mass of the 95% CH_4 cases (up) and the 99% CH_4 cases (down).

consume 6.8 kW/MW_e, while cases at 10 bar consume 29.6 kW/MW_e (Cases #95P, #99P and #Z).

The reactor volume is directly proportional to the catalyst mass required. A minimum mass of 12.4 kg/MW_e is obtained for the case #4 (without technical constraints). Nonetheless, considering a maximum GHSV of 5000 h^{-1}, the required mass is higher, as it is evidenced in the cases with technical limits. The catalyst mass further increases for the #99 cases, as they require higher purities and therefore more reactors.

The zeolite SEM case presents the highest catalyst consumption of all configurations (223.7 kg/MW_e), even though it operates at similar GHSV (~4400 h^{-1}) and there are no reactors in series (methanation occurs in 1 stage). The reason behind this is the fact that SEM uses 4 reactors in parallel (1 methanizing and 3 desorbing water), so each of the reactor has 55.9 kg_{cat}/MWe. This amount of catalyst is similar to the one contained in the 1st reactor of CM constrained configurations, where most of the conversion occurs (see Fig. 10, cases #3C, #95P, #99P and #99A). Thus, while SEM needs to replicate this 1st reactor 4 times (because they operate alternatively every 15 min), the CM just needs to add reactors in series with much less catalyst amount to marginally increase the CH_4 purity. Even in the case #99A (Fig. 10), the total amount of catalyst contained within the 2nd to the 13th reactor (144.8 kg_{cat}/MW_e) is not as big as the amount contained in the 3 other parallel reactors needed in SEM (167.7 kg_{cat}/MW_e).

4.4. Economic KPIs

The economic results are summarized in CAPEX, OPEX, incomes, specific implementation cost and levelized cost of methane (Table 7). In terms of CAPEX, the cost of the reactors is the main driver (therefore, differences in the zeolite and filler cost are not relevant). Looking at the 95 vol% CH_4 purity cases, the cases with technical restrictions are more expensive, since the minimum GHSV is limiting the minimum size of the reactors. Therefore, they are oversized in comparison with the cases without technical restrictions (#2, #3, #4), whose capital costs decrease as the number of reactors increases, due to the smaller size of them, offsetting the higher reactor count. Additionally, the increased cost of the #95P reactors due to the necessity of withstanding higher pressures offsets the benefit of having only two, presenting the highest CAPEX of the 95% cases. Regarding the 99% CH_4 cases, the #99A presents the highest costs, as it involves 13 series reactors. The effect of the increased pressure can also be directly compared between #99P and the #3C case, as both cases present 3 reactors and similar total mass catalyst. The zeolite SEM case presents a moderate capital investment, somewhat comparable with the #99P case.

Regarding the operational costs indicated in Table 7, the main responsible for all cases is the cost of the hydrogen, reaching up to 96% of the OPEX for the case #2. The relative contribution decreases in the CAPEX-heavy cases, as the O&M costs are directly related to the capital investment. Still, hydrogen contribution to the OPEX decreases only to a minimum value of 88 % for the #99A case. Third contributor is electricity, whereas the influence of the rest of the elements are negligible. It is worth mentioning that the additional H_2 used in the regeneration gas in the zeolite SEM case is not accounted, as it is operating in a closed loop.

Incomes are divided in CO_2 taxes (savings) and CH_4 sold. The income related with the CO_2 tax is the same in all cases, as it is directly related to the inlet CO_2 and CO flows. The income related to the SNG sell shows a great difference as CH_4 purity increases. Therefore, the incomes of the zeolite SEM case are 3 times higher than the 99% cases, which are themselves 6 times greater than the 95% cases.

The specific implementation cost (SIC), calculated as indicated in Table 2 and is similar for all the 95% cases, approximately constant at 1.5 €/kg_{SNG} (Fig. 11). Among them, the technical limited cases (#3C, and specially #95P) present a slightly higher cost due do the higher

Table 6
Comparison of global technical KPIs between CM and SEM. *Cooling at 0 °C (it requires refrigeration).

Global KPI	#2	#3	#4	#3C	#95P	#99P	#99A	#Z
Heating (covered by integration) (kW/MW_e)	43.9	62.9	85.4	90.0	40.4	51.0	162.8	23.08
Cooling (reactors) (kW/MW_e)	168.4	169.4	170.4	170.4	167.5	168.8	169.6	174.8
Cooling (condensers) (kW/MW_e)	80.1	97.9	119.4	119.4	74.1	89.7	206.4*	64.5
Electricity consumption (kW/MW_e)	10.7	8.7	8.7	8.3	30.3	30.2	42.9	34.2
Electric heating (kW/MW_e)	3.9	1.9	1.9	1.5	0.7	0.6	17.2	4.56
Refrigeration (kW/MW_e)	0	0	0	0	0	0	18.9	0
Compressor work (kW/MW_e)	6.8	6.8	6.8	6.8	29.6	29.6	6.8	29.6
m_{cat} (total) (kg/MW_e)	69.4	20.4	12.4	78.3	70.4	91.0	195.5	223.7
Volume (total) (l/MW_e)	173.5	50.9	30.9	195.7	176.0	187.0	488.8	718.0

Table 7
Breakdown of CAPEX, OPEX and incomes of each case, assuming 200 MWe electrolyzer.

	#2	#3	#4	#3C	#95P	#99P	#99A	#Z
Purity (CH_4 vol% d.b.)	95	95	95	95	95	99	99	100
CAPEX (M€)	**298.03**	**155.39**	**121.05**	**354.76**	**598.74**	**693.62**	**1081.3**	**805.46**
Process direct costs								
Reactors	83.59	43.22	33.06	100.35	170.65	198.18	308.37	227.46
Compressor	0.82	0.82	0.82	0.82	2.21	2.21	0.82	2.21
Preheaters	0.96	0.63	0.88	0.53	0.14	0.17	1.72	0.77
Condensers	0.20	0.25	0.29	0.25	0.23	0.25	0.64	0.13
Catalyst	1.30	0.38	0.24	1.46	1.32	1.4	3.67	4.20
Filler	0.02	<0.01	<0.01	0.01	0.01	0.01	0.04	0
Zeolite	0	0	0	0	0	0	0	0.07
Other direct costs	118.17	61.61	48.00	140.66	237.40	275.02	428.73	319.36
Indirect costs	92.97	48.48	37.76	110.67	186.78	216.38	337.31	251.26
OPEX (M€/y)	**203.76**	**200.34**	**199.60**	**204.74**	**212.21**	**214.23**	**224.11**	**217.07**
Hydrogen	196.03	196.03	196.03	196.03	196.03	196.03	196.03	196.03
Electricity	1.13	0.91	0.92	0.88	3.20	3.19	4.36	3.13
Catalyst renovation	0.20	0.06	0.03	0.22	0.20	0.21	0.55	0.63
Filler renovation	<0.01	<0.01	<0.01	<0.01	<0.01	<0.01	0.01	0
Zeolite renovation	0	0	0	0	0	0	0	0.01
O&M	8.94	4.66	3.63	10.64	17.96	20.81	32.44	24.16
INCOMES (M€/y)	**54.57**	**54.57**	**54.57**	**54.57**	**54.57**	**340.30**	**340.30**	**943.88**
CO_2 taxes	15.53	15.53	15.53	15.53	15.53	15.53	15.53	15.53
CH_4 sold	39.04	39.04	39.04	39.04	39.04	324.77	324.77	928.35
SIC (€/kg_{SNG})	1.47	1.34	1.31	1.52	1.76	−0.61	−0.24	−5.80
LCOM (€/kg_{SNG})	2.65	2.46	2.42	2.73	3.30	3.04	3.85	3.46

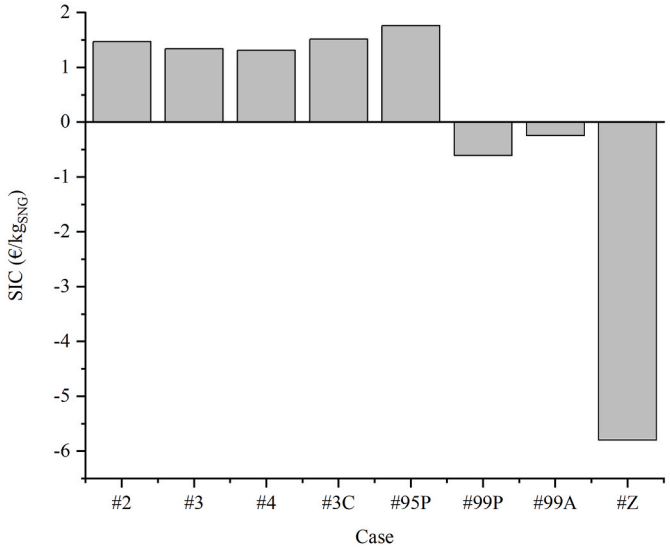

Fig. 11. Specific implementation cost (SIC) of the studied cases.

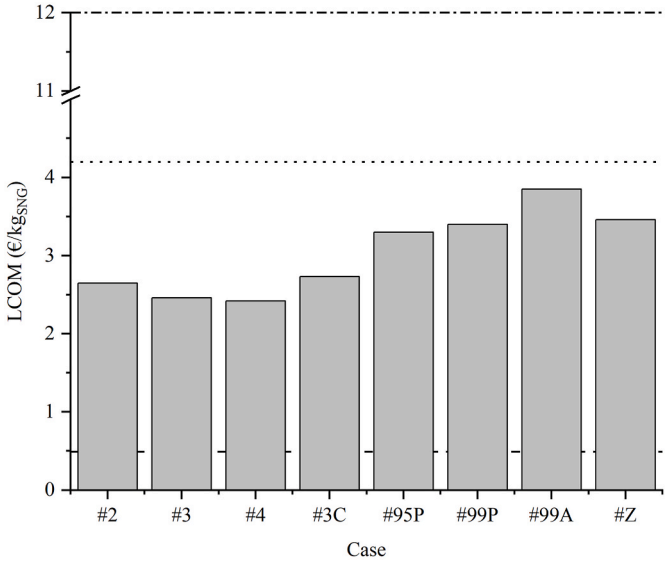

Fig. 12. Levelized cost of methane (LCOM) of the studied cases.

CAPEX. The greater revenue obtained from the higher purity SNG in the 99% cases allows for them to achieve negative SICs of −0.6 and −0.2 €/kg_{SNG}, despite their higher capital costs. A negative SIC means that the integration is profitable. The #99A case is less competitive than the #99P, due to the reactor investment. Finally, the zeolite SEM case presents the best economic results. The CAPEX is comparable to the 99% ones, but the really high SNG-related revenue, thanks to the superior quality of the obtained gas, allows obtaining a SIC of −5.8 €/kg_{SNG}.

Regarding the Levelized Cost of Methane, it represents the cost of production of methane. Therefore, when the LCOM is lower than the market cost, the integration is profitable. In Fig. 12, the LCOM is compared against the market cost of the methane of each purity. The same conclusions can be extrapolated as for the SIC. The 95% cases represent economic losses since the production cost by methanation (2.4 – 3.3 €/kg_{SNG}) cannot compete with the current market price of natural gas (0.5 €/kg_{CH4}). When the SNG reaches 99% purity, it might be profitable as these cases present LCOMs (3.0 – 3.9 €/kg_{SNG}) slightly lower than the current market price for this purity (4.2 €/kg_{SNG}). In the case of SEM, although the LCOMs is similar (3.5 €/kg_{SNG}) it can access to a premium market for 99.9% high-purity methane with a market price of 12 €/kg_{CH4}. Therefore, even considering potential uncertainties in the techno-economic assessment (like the additional costs that may appear at such high purities for post-processing, which were not considered), it can be concluded that SEM would be profitable in this market.

For the aim of a more thoroughly discussion, the influence of different parameters is assessed in Fig. 13, which shows how a ±50% variation in these parameters affects the final levelized cost of methane. The cost of hydrogen is clearly the biggest source of uncertainty, followed by the cost of reactors, and the part of the CAPEX that is not related with the equipment (i.e., other direct costs plus indirect costs). Smaller influences are found in the carbon tax and in the interest rate. Lastly, a variation in the cost of electricity has no effect in the LCOM. This is because we only account electricity for compressors and some preheating, and not for H_2 production (which has its own cost).

Subsequently, specific sensitivity analyses on the reactor unitary

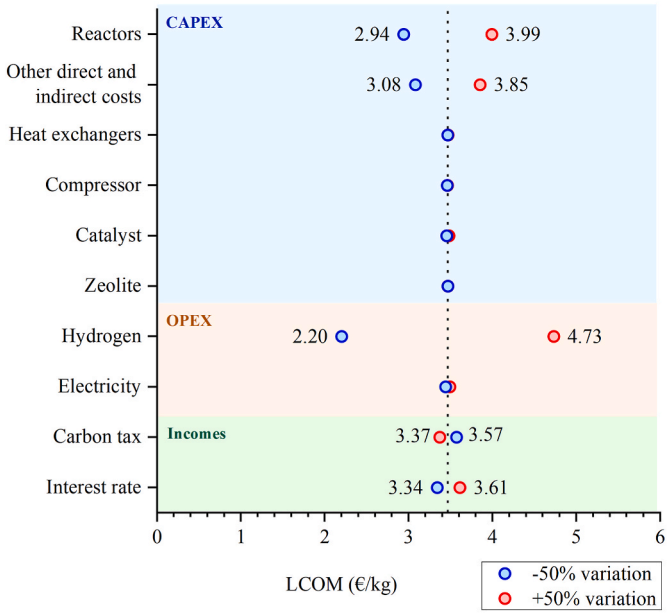

Fig. 13. Sensitivity analysis on the effect of different economic assumptions (±50% variation) over the LCOM (for case #Z, sorption-enhanced methanation).

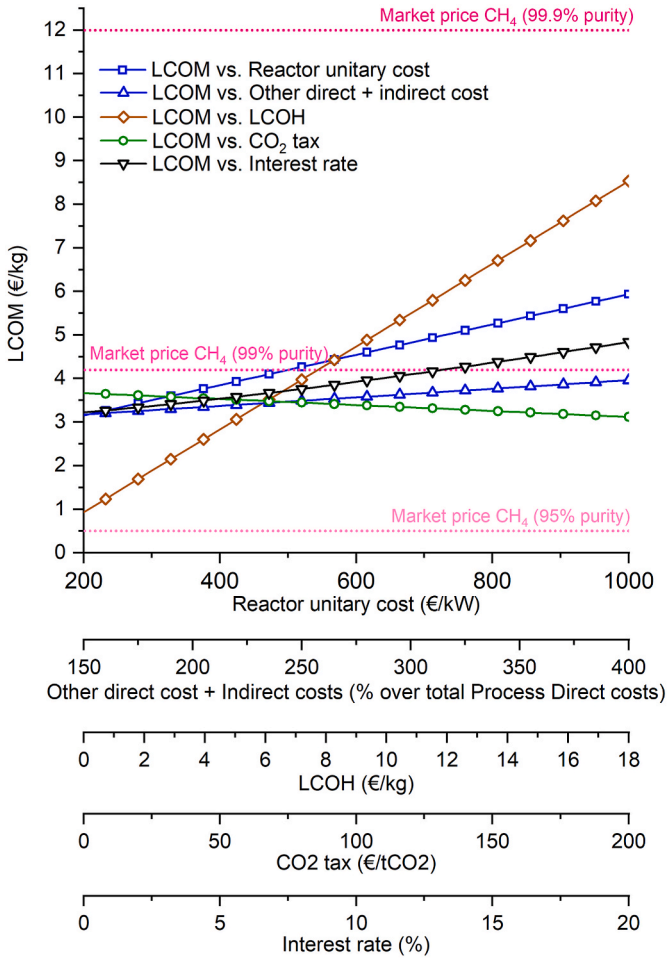

Fig. 14. Sensitivity analysis on the five economic parameters that most influence the LCOM (for case #Z, sorption-enhanced methanation).

cost, the other CAPEX, the hydrogen cost, the CO_2 tax and the interest rate are conducted (Fig. 14). In all cases, it is not possible to compete in the market of 95% purity methane, since the LCOM is always above the market price. Contrarily, even in the most unfavorable scenarios, participating in the market of 99.9% purity CH_4 is always profitable. If we want to access to a larger market share, by competing in the 99% purity CH_4 market, some of the economic parameters should be controlled.

The reactor unitary cost is varied from 200 €/kW to 1000 €/kW (base case is 423 €/kW), posing conservative scenarios. Results show that the reactor cost should be below 500 €/kW if we want to be profitable in both the 99% and 99.9% purity markets. Regarding the other CAPEX, there is a margin large enough within which the operation remains profitable in both markets. Even a scenario in which the other CAPEX (direct cost plus indirect costs) represent the 400% of the process direct cost (base case scenario is 243%), the levelized cost of methane only increases by 14%, resulting in 3.96 €/kg, which is below the 99% purity CH_4 market price of 4.2 €/kg.

Hydrogen is the main and most expensive input to the system, so its cost is the most sensitive parameter. The sensitivity analysis considered costs from 0 €/kg_{H2} to 18 €/kg_{H2}. The former represents a scenario in which H_2 comes for free as by-product from an industry (e.g., during chlorine production [69]), while the latter is green H_2 produced at extremely high cost through non-mature technologies like photo-catalytic water splitting, bio-photolysis or photoelectrochemical water splitting [70]. This wide range of costs covers the 2022 price [71] for all types of hydrogen generation: black and grey (1.25 €/kg), blue (2 to 7 €/kg), pink (3.5 to 7 €/kg) and green H_2 (up to 12 €/kg). Results show that the levelized cost of H_2 should be below 7.8 €/kg to be competitive in the 99% purity CH4 market, what means that some configurations based on green H_2 might be limited to participate only in the 99.9% purity market. Surprisingly, even considering cost-free H_2, profitability in the market of 95% purity CH_4 is not reachable. The good thing is that sorption-enhanced methanation can always compete in the 99.9% purity market, what may help innovative H_2 production technologies to become mature under profitable scenarios.

Regarding the CO_2 tax, the results showed that CH_4 production by SEM is profitable even if no savings associated to CO_2 utilization are considered, obtaining a LCOM of 3.67 €/kg. Consequently, a favorable carbon credit market of 200 €/t_{CO2} reduces the LCOM moderately by 15%, resulting in 3.12 €/kg, what increases the benefits but not the market possibilities.

The yearly interest rate (or discount rate) is varied from 0% to 20%, which are both extreme scenarios. This variation only modifies the LCOM from 3.22 €/kg to 4.84 €/kg, what means that the 99% purity CH_4 market is profitable for interest below 13.2%.

5. Conclusions

This work presented the first techno-economic assessment of sorption-enhanced methanation, benchmarked against conventional methanation. Both technologies were modelled in Aspen Plus based on experimental data (TRL-3), using a mixture of 60 vol% CO and 40 vol% CO_2 (typical of the ironmaking industry). The sorption-enhanced methanation comprised four reactors filled with catalyst and adsorbent, alternating methanation (15 min) and regeneration stages (45 min), so SNG production was continuous. In the case of conventional methanation, different configurations were considered, aiming for 95 or 99 vol% CH_4, at 1 or 10 bar. These were optimized to minimize the amount of catalyst used, considering technical constrains typical of industrial plants (GHSV $\leq$5000 h^{-1}, and $\geq$300 °C).

In the experiments, a fixed-bed configuration was used (20 g of Nickel-based catalyst, mixed with 80 g of zeolite 4A –SEM– or SiC –CM–). For conventional methanation, the CO_2 conversion ranged from 73.2% to 95.9% (performed at 5 to 10 bar and >250 °C). The maximum purity of CH_4 was 93.9 vol% d.b., which is consistent with

thermodynamic predictions (95.8 vol% d.b.). The SEM experiments resulted in 100 vol% CH_4 purity, thanks to the in-situ adsorption of H_2O by the zeolite, producing 0.016 mol_{CH4}/kg_{cat}·s.

These tests were used to fit a kinetic model (±10% error), used later to size the reactors in the different plant configurations of the techno-economic analysis. In conventional methanation, the needed catalyst mass was around 50 kg_{cat}/MW_e in the first reactor and tend to decrease in the followings, resulting in 70 – 90 kg_{cat}/MW_e in total (considering only the most reasonable layouts). The SEM case presented the highest catalyst consumption (223.7 kg/MW_e), even though it operates at similar GHSV (~4400 h^{-1}). The reason behind this is the fact that SEM used 4 reactors in parallel (1 methanizing and 3 desorbing water), so each of the reactor contained 55.9 kg_{cat}/MWe (similar to the first reactor in conventional methanation).

The economic results were reported for a plant size of 200 MW_e in line with some of the major ongoing projects. In terms of CAPEX, the cost of the reactors was the main driver. When operating methanation at 10 bar and 99% CH_4, both SEM and CM presented a similar capital investment (~700-800 M€). Regarding the operational costs, the main driver was the cost of the hydrogen, representing 88% to 96% of the OPEX (196 M€/y). The main difference was due to income related to the sale of SNG. It showed a great difference as CH_4 purity increases (55 M€/y for 95% CH_4, 340 M€/y for 99% CH_4, and 944 M€/y for 99.9% CH_4). Therefore, the incomes of the SEM case are 3 times higher than the 99% cases of CM, and 17 times greater than the 95% cases.

For the sake of discussion, the levelized cost of methane was chosen as indicator. It represents the cost of production of the methane, and must be lower than the market price to obtain profits. The 95% purity cases, in CM, led to economic losses since the production cost by methanation (2.4 – 3.3 €/kg_{SNG}) cannot compete with the current market price of natural gas (0.5 €/kg_{CH4}). When the SNG reached 99% purity in CM, profits may be possible as these cases presented LCOMs (3.0 – 3.9 €/kg_{SNG}) slightly lower than the current market price for this purity (4.2 €/kg_{SNG}). In the case of SEM, the LCOM (3.5 €/kg_{SNG}) is similar to CM, but sorption-enhanced methanation can access to a premium market for 99.9% CH_4 (12 €/kg_{CH4}), thus guaranteeing profits.

Once concluded the economic advantages of SEM against CM, a sensitivity analysis for SEM was performed. The cost of hydrogen was clearly the biggest source of uncertainty, followed by the cost of reactors. Whatever the scenario was (even considering free H_2), competing in the market of 95% purity methane was not possible for SEM, since the LCOM was always above the market price. In order to compete in the 99% purity CH_4 market, and so accessing to a larger share of potential clients, the reactor cost should be below 500 €/kW. Moreover, the levelized cost of the H_2 that is consumed should be below 7.8 €/kg_{H2}, what means that some configurations based on green H_2 might be not adequate. Nevertheless, even in the most unfavorable scenarios (e.g., LCOH of 18€/kg_{H2}), participating in the market of 99.9% purity CH_4 was always profitable. Therefore, sorption-enhanced methanation may help other innovative H_2 production technologies to become mature under profitable scenarios, since SEM can always compete in the 99.9% purity CH_4 market.

Nomenclature

C	Capital expenditure	M€
COP_{carnot}	Theoretical coefficient of performance (Carnot cycle)	-
$E_{A,j}$	Activation energy of reaction "j"	J/mol
F	Specific volumetric flow	m^3/h-MW
GHSV	Gas Hourly Space Velocity	h^{-1}
ΔH_i^0	Enthalpy of adsorption of component "i"	J/mol
I	Income	M€/y
K_i	Adsorption constant of component "i"	See Table 4
$K_{eq,1}$	Equilibrium constant of reaction 1	-
$K_{eq,2}$	Equilibrium constant of reaction 2	Pa^2
k_j	Rate coefficient of reaction "j"	See Table 4
LCOM	Levelized cost of methane	€/kg_{SNG}
M_{MSE}	Arithmetic mean of MSE_i	-
MSE_i	Mean squared error of volumetric concentration of component "i"	-
m_{fill}	Filler mass	kg/MW_e
m_{cat}	Catalyst mass	kg/MW_e
$m_{SNG,20years}$	SNG production during 20 years of operation	t
$\dot{m}_i$	Specific mass flow of component "I"	kg/h-MW_e
NPV	Net Present Value	M€
$\dot{n}_i$	Molar flow of component "i"	kmol/h-MW_e
O	Operational expenditure	M€/y
p_i	Partial pressure of component "i"	Pa
q	Specific heat	kW/MW_e
r_j	Kinetic rate of reaction "j"	mol/g_{cat}-s
R	Universal constant	J/mol-K
S_{CH4}	CH_4 selectivity	%
SIC	Specific Implementation Cost	€/kg_{SNG}
T	Temperature	°C[a]
v	Specific volume	l/MW_e
w_{comp}	Specific compressor work	kW/MW_e
X_{CO2}	CO_2 conversion	%
x_i	Volumetric concentration of component "i"	-
ρ	Density	kg/m^3

[a] Except for calculation of $E_{a,j}$, where it is measured in Kelvin.

CRediT authorship contribution statement

C. Barón: Writing – original draft, Visualization, Software, Methodology, Conceptualization. **L. Gómez:** Writing – original draft, Visualization, Validation, Investigation, Conceptualization. **I. Martínez:** Writing – original draft, Validation, Supervision, Resources, Project administration, Investigation, Funding acquisition, Conceptualization. **M. Bailera:** Writing – review & editing, Writing – original draft, Visualization, Supervision, Software, Resources, Project administration, Methodology, Funding acquisition, Conceptualization.

Data statement

Experimental data is available in the supplementary material.

Declaration of competing interest

The authors declare that they have no known competing financial interests or personal relationships that could have appeared to influence the work reported in this paper.

Acknowledgements

The authors acknowledge the project PID2021-123878OBI00 funded by MICIN/AEI/10.13039/501100011033 and FEDER "A way of making Europe", as well as the Regional Government of Aragon (DGA) under the Research Groups Support Programme. Laura Gómez Alonso also thanks DGA for the postdoctoral research grant received (EMC/191/2025), awarded within the Odón de Buen program. This publication is also supported by RYC2022-038283-I, funded by MCIN/AEI/10.13039/501100011033 and the European Social Fund Plus (FSE+), and by Government of Aragon (Research Group DGA T46_17R). This article is part of the R&D project PID2023-149968OB-I00, funded by MICIU/AEI/10.13039/501100011033/and by FEDER, UE. The FPU Programme of the Spanish Ministry of Science, Innovation and Universities (FPU/00073) provided financial support for Cristian Barón PhD studies. Aspen Technology Inc is also acknowledged for the use of the software.

Appendix A. Supplementary data

Supplementary data to this article can be found online at https://doi.org/10.1016/j.ijhydene.2026.154958.

References

[1] Gabrielli P, Gazzani M, Mazzotti M. The role of carbon capture and utilization, carbon capture and storage, and biomass to enable a Net-Zero-CO_2 emissions chemical industry. Ind Eng Chem Res 2020;59:7033–45. https://doi.org/10.1021/acs.iecr.9b06579.

[2] IPCC. Global warming of 1.5°C: headline statements from the summary for policymakers. Global warming of 15°C an IPCC special report on the impacts of global warming of 15°C above pre-industrial levels and related global greenhouse gas emission pathways. In: The context of strengthening the global response to the threat of climate change; 2018. p. 1–2.

[3] Pastor-Pérez L, Saché E Le, Jones C, Gu S, Arellano-Garcia H, Reina TR. Synthetic natural gas production from CO_2 over Ni-x/Ce_{O2}-Zr_{O2} (x = Fe, Co) catalysts: influence of promoters and space velocity. Catal Today 2018;317:108–13. https://doi.org/10.1016/j.cattod.2017.11.035.

[4] Mustafa A, Lougou BG, Shuai Y, Wang Z, Tan H. Current technology development for CO_2 utilization into solar fuels and chemicals: a review. J Energy Chem 2020;49:96–123. https://doi.org/10.1016/j.jechem.2020.01.023.

[5] Peres CB, Resende PMR, Nunes LJR, Morais LC de. Advances in carbon capture and use (CCU) technologies: a comprehensive review and CO_2 mitigation potential analysis. Cleanroom Technol 2022;4:1193–207. https://doi.org/10.3390/cleantechnol4040073.

[6] Walspurger S, Haije WG, Louis B. CO_2 reduction to substitute natural gas: toward a global low carbon energy system. Isr J Chem 2014;54:1432–42. https://doi.org/10.1002/ijch.201300135.

[7] Rosa R. The role of synthetic fuels for a carbon neutral economy. C (Basel) 2017;3:11. https://doi.org/10.3390/c3020011.

[8] Fetting C. The European green deal. ESDN Report 2020;53:24. European Commission.

[9] Reiter G, Lindorfer J. Global warming potential of hydrogen and methane production from renewable electricity via power-to-gas technology. Int J Life Cycle Assess 2015;20:477–89. https://doi.org/10.1007/s11367-015-0848-0.

[10] Jaffar MM, Nahil MA, Williams PT. Parametric study of CO_2 methanation for synthetic natural gas production. Energy Technol 2019;7. https://doi.org/10.1002/ente.201900795.

[11] Rönsch S, Schneider J, Matthischke S, Schlüter M, Götz M, Lefebvre J, et al. Review on methanation - from fundamentals to current projects. Fuel 2016;166:276–96. https://doi.org/10.1016/j.fuel.2015.10.111.

[12] Bailera M, Lisbona P, Romeo LM, Espatolero S. Power to gas projects review: lab, pilot and demo plants for storing renewable energy and CO_2. Renew Sustain Energy Rev 2017;69:292–312. https://doi.org/10.1016/j.rser.2016.11.130.

[13] Bailera M, Peña B, Lisbona P, Marín J, Romeo LM. Lab-scale experimental tests of power to gas-oxycombustion hybridization: system design and preliminary results. Energy 2021;226. https://doi.org/10.1016/j.energy.2021.120375.

[14] Kopyscinski J, Schildhauer TJ, Biollaz SMA. Production of synthetic natural gas (SNG) from coal and dry biomass - a technology review from 1950 to 2009. Fuel 2010;89:1763–83. https://doi.org/10.1016/j.fuel.2010.01.027.

[15] Ghaib K, Nitz K, Ben-Fares FZ. Chemical methanation of CO_2: a review. ChemBioEng Rev 2016;3:266–75. https://doi.org/10.1002/cben.201600022.

[16] Gao J, Wang Y, Ping Y, Hu D, Xu G, Gu F, et al. A thermodynamic analysis of methanation reactions of carbon oxides for the production of synthetic natural gas. RSC Adv 2012;2:2358–68. https://doi.org/10.1039/c2ra00632d.

[17] Bartholomew CH. Mechanisms of catalyst deactivation. Appl Catal Gen 2001;212:17–60. https://doi.org/10.1016/S0926-860X(00)00843-7.

[18] Bolt A, Dincer I, Agelin-Chaab M. A critical review of synthetic natural gas production techniques and technologies. J Nat Gas Sci Eng 2020;84:103670. https://doi.org/10.1016/j.jngse.2020.103670.

[19] Aziz MAA, Jalil AA, Triwahyono S, Ahmad A. CO_2 methanation over heterogeneous catalysts: recent progress and future prospects. Green Chem 2015;17:2647–63. https://doi.org/10.1039/c5gc00119f.

[20] Meloni E, Cafiero L, Renda S, Martino M, Pierro M. Ru- and Rh-Based catalysts for CO_2 methanation assisted by non-thermal plasma. Journal of Catalysts 2023;13.

[21] Sanz-Martínez A, Durán P, Mercader VD, Francés E, Peña JÁ, Herguido J. Biogas upgrading by CO2 methanation with Ni-, Ni–Fe-, and Ru-Based catalysts. Catalysts 2022;12. https://doi.org/10.3390/catal12121609.

[22] Lee WJ, Li C, Prajitno H, Yoo J, Patel J, Yang Y, et al. Recent trend in thermal catalytic low temperature CO_2 methanation: a critical review. Catal Today 2021;368:2–19. https://doi.org/10.1016/j.cattod.2020.02.017.

[23] Schaaf T, Grünig J, Schuster MR, Rothenfluh T, Orth A. Methanation of CO_2 - storage of renewable energy in a gas distribution system. Energy Sustain Soc 2014;4:1–14. https://doi.org/10.1186/s13705-014-0029-1.

[24] Borgschulte A, Gallandat N, Probst B, Suter R, Callini E, Ferri D, et al. Sorption enhanced CO_2 methanation. Phys Chem Chem Phys 2013;15:9620–5. https://doi.org/10.1039/c3cp51408k.

[25] Delmelle R, Duarte RB, Franken T, Burnat D, Holzer L, Borgschulte A, et al. Development of improved nickel catalysts for sorption enhanced CO_2 methanation. Int J Hydrogen Energy 2016;41:20185–91. https://doi.org/10.1016/j.ijhydene.2016.09.045.

[26] Walspurger S, Haije WG, Louis B. CO_2 reduction to substitute natural gas: toward a global low carbon energy system. Isr J Chem 2014;54:1432–42. https://doi.org/10.1002/ijch.201300135.

[27] van Kampen J, Boon J, van Berkel F, Vente J, van Sint Annaland M. Steam separation enhanced reactions: review and outlook. Chem Eng J 2019;374:1286–303. https://doi.org/10.1016/j.cej.2019.06.031.

[28] Gómez L, Martínez I, Navarro MV, García T, Murillo R. Sorption-enhanced CO and CO_2 methanation (SEM) for the production of high purity methane. Chem Eng J 2022;440:135842. https://doi.org/10.1016/j.cej.2022.135842.

[29] Stangeland K, Kalai D, Li H, Yu Z. CO_2 methanation: the effect of catalysts and reaction conditions. Energy Proc 2017;105:2022–7. https://doi.org/10.1016/j.egypro.2017.03.577.

[30] Catarina Faria A, Miguel CV, Madeira LM. Thermodynamic analysis of the CO_2 methanation reaction with in situ water removal for biogas upgrading. J CO2 Util 2018;26:271–80. https://doi.org/10.1016/j.jcou.2018.05.005.

[31] Roque-Malherbe R. Complementary approach to the volume filling theory of adsorption in zeolites. Microporous Mesoporous Mater 2000;41:227–40. https://doi.org/10.1016/S1387-1811(00)00296-1.

[32] Delmelle R, Terreni J, Remhof A, Heel A, Proost J, Borgschulte A. Evolution of water diffusion in a sorption-enhanced methanation catalyst. Catalysts 2018;8:1–15. https://doi.org/10.3390/catal8090341.

[33] Borgschulte A, Delmelle R, Duarte RB, Heel A, Boillat P, Lehmann E. Water distribution in a sorption enhanced methanation reactor by time resolved neutron imaging. Phys Chem Chem Phys 2016;18:17217–23. https://doi.org/10.1039/c5cp07686b.

[34] Wei L, Azad H, Haije W, Grenman H, de Jong W. Pure methane from CO_2 hydrogenation using a sorption enhanced process with catalyst/zeolite bifunctional materials. Appl Catal, B 2021;297:120399. https://doi.org/10.1016/j.apcatb.2021.120399.

[35] Walspurger S, Elzinga GD, Dijkstra JW, Sarić M, Haije WG. Sorption enhanced methanation for substitute natural gas production: experimental results and thermodynamic considerations. Chem Eng J 2014;242:379–86. https://doi.org/10.1016/j.cej.2013.12.045.

[36] Mannschreck R, Agirre I. Sorption enhanced methanation: a study on reactor configuration and sorption effects on the sabatier process. Nevada State Undergraduate Research Journal 2019;5:40–5. https://doi.org/10.15629/6.7.8.7.5_5-1_S-2019_5.

[37] Agirre I, Acha E, Cambra JF, Barrio VL. Water sorption enhanced CO_2 methanation process: optimization of reaction conditions and study of various sorbents. Chem Eng Sci 2021;237:116546. https://doi.org/10.1016/j.ces.2021.116546.

[38] Gómez L, Martínez I, Navarro MV, Murillo R. Selection and optimisation of a zeolite/catalyst mixture for sorption-enhanced CO_2 methanation (SEM) process. J CO2 Util 2023;77:102611. https://doi.org/10.1016/j.jcou.2023.102611.

[39] Gómez L, Martínez I, Grasa G, Murillo R. Experimental demonstration of a sorption-enhanced methanation (SEM) cyclic process on a lab-scale TRL-3 fixed bed reactor. Chem Eng J 2024;491:151744. https://doi.org/10.1016/j.cej.2024.151744.

[40] Gómez L, Martínez I, Grasa G, Murillo R. Study of different feed mixtures for the sorption-enhanced methanation (SEM) process on a lab-scale TRL-3 fixed-bed reactor. Energy Fuels 2024;38:17834–46. https://doi.org/10.1021/acs.energyfuels.4c02622.

[41] Bailera M, Lisbona P, Peña B, Romeo LM. A review on CO_2 mitigation in the iron and steel industry through power to X processes. J CO2 Util 2021;46:101456. https://doi.org/10.1016/j.jcou.2021.101456.

[42] Qu Y, Zou Z, Xiao Y. A comprehensive static model for COREX process. ISIJ Int 2012;52:2186–93. https://doi.org/10.2355/isijinternational.52.2186.

[43] Wu S, Xu J, Yagi J, Guo X, Zhang L. Prediction of pre-reduction shaft furnace with top gas recycling technology aiming to cut Down CO_2 emission. ISIJ Int 2011;51:1344–52. https://doi.org/10.2355/isijinternational.51.1344.

[44] Bonacina CN, Romano MC, Colbertaldo P, Milocco A, Valenti G. Techno-economic study of chimneyless electric arc furnace plants for the coproduction of steel and of electricity, hydrogen, or methanol. J Clean Prod 2024;468:143048. https://doi.org/10.1016/j.jclepro.2024.143048.

[45] IEA. Outlook for Biogas and biomethane. 2025.

[46] Air liquide https://uk.airliquide.com/solutions/biogas-waste-renewable-energy.

[47] Josef gases https://josefgases.com/gas/methane-specialty-gas/.

[48] IndustryARC. High Purity Methane Gas Market – By Purity Level , By Form , By Production Method , By Application , By End-User , By Geography – Global Opportunity Analysis & Industry Forecast, 2025-2031.

[49] Krenn A, Stewart M, Mitchell D, Dixon K, Mierzwa M, Breon S. Flight servicion of robotic Refueling Mission 3.

[50] Bailera M, Lisbona P, Peña B, Romeo LM. Energy storage. Cham: Springer International Publishing; 2020.

[51] Peña B, Bailera M, Legaz J, Barón C, Garlatti S, Zampilli M, et al. Development, testing, performance analysis and modelling of a biochar-based catalyst for methanation reaction. Renew Energy 2025;250:123248. https://doi.org/10.1016/j.renene.2025.123248.

[52] Goméz L, Nguyen-Quang M, Azzolina-Jury F, Martínez I, Murillo R. In-situ FTIR analysis on conventional and sorption-enhanced methanation (SEM) processes over Ni, Rh, and Ru-based catalyst systems. Appl Catal Gen 2024;678:119733. https://doi.org/10.1016/j.apcata.2024.119733.

[53] Gómez L, Grasa G, Martínez I, Murillo R. Performance study of a methanation process for a syngas obtained from a sorption enhanced gasification process. Chem Eng Sci 2023;267:118291. https://doi.org/10.1016/j.ces.2022.118291.

[54] Bartik A, Fuchs J, Pacholik G, Föttinger K, Hofbauer H, Müller S, et al. Experimental investigation on the methanation of hydrogen-rich syngas in a bubbling fluidized bed reactor utilizing an optimized catalyst. Fuel Process Technol 2022;237:107402. https://doi.org/10.1016/j.fuproc.2022.107402.

[55] Jianguo X, Froment GF. Methane steam reforming , methanation and water-gas shift : 1. Intrinsic Kinetics 1989;35.

[56] Vassiliadis VS, Conejeros R. Powell method. In: Encyclopedia of optimization; 2008.

[57] Saint M De, Baurens P, Bouallou C, Couturier K. Economic assessment of a power-to-substitute- natural-gas process including high-temperature steam electrolysis. Int J Hydrogen Energy 2015;40:6487–500. https://doi.org/10.1016/j.ijhydene.2015.03.066.
[58] https://67d762fd1f819b6a.en.made-in-china.com/product/jnSYMKNlyChV/China-Industrial-Grade-4A-Zeolite-for-Washing-Additives-Used-in-Super-Concentrated-Washing-Powder.html?header_search_page=lv.
[59] https://www.lme.com/en/Metals/Non-ferrous/LME-Alumina_#Trading+day+summary.
[60] Lehner M, Tichler R, Steinmüller H, Koppe M. Power-to-gas: technology and business models. Springler Briefs in Energy 2014. https://doi.org/10.1007/978-3-319-03995-4.
[61] Turton R, Bailie R, Whiting WB, Shaeiwitz J, Bhattacharyya D. Analysis, synthesis, and design of chemical processes. Fourth. Prentice Hall; 2012.
[62] International IEA, Agency E. Global Hydrogen Review 2023. 2023.
[63] N.d. https://tradingeconomics.com/spain/electricity-price.
[64] n.d. https://www.mibgas.es/es.
[65] n.d. https://www.tradeindia.com/products/ultra-high-purity-uhp-coal-gas-industrial-methane-gas-8075950.html.
[66] n.d. https://tyhjgas.en.made-in-china.com/product/BOvaMZhPlUfo/China-Specialty-Gas-99-99-Purity-Methane-CH4-Gas-Cylinder-Price-Per-Cylinder.html.
[67] N.d. https://www.man-es.com/company/press-releases/press-details/2023/08/17/man-energy-solutions-wins-pre-engineering-contract-for-methanation-reactor-in-power-to-x-plant.
[68] Gómez L, Isabel M, Murillo R. Biogas-to-Methane conversion via sorption-enhanced methanation: experimental evaluation of reactor configuration strategies Under Revision in Applied Energy.
[69] Bailera M, Espatolero S, Lisbona P, Romeo LM. Power to gas-electrochemical industry hybrid systems: a case study. Appl Energy 2017;202:435–46. https://doi.org/10.1016/j.apenergy.2017.05.177.
[70] Frowijn LSF, van Sark WGJHM. Analysis of photon-driven solar-to-hydrogen production methods in the Netherlands. Sustain Energy Technol Assessments 2021;48:101631. https://doi.org/10.1016/j.seta.2021.101631.
[71] - International Energy Agency I. Global Hydrogen Review 2023. 2023.